Polar Geosci., **19**, 1–36, 2006
© 2006 National Institute of Polar Research

Geology of Byôbu Rock and Gobanme Rock, Prince Olav Coast, East Antarctica

M. Satish-Kumar[1]*, Shin-ichi Kagashima[2], Yoshimitsu Suda[3] and Yoichi Motoyoshi[3]

[1]*Institute of Geosciences, Shizuoka University, Oya 836, Suruga-ku, Shizuoka 422-8529*
[2]*Department of Earth and Environmental Sciences, Faculty of Science, Yamagata University, Kojirakawa-machi 1–4–12, Yamagata 990-8560*
[3]*National Institute of Polar Research, Kaga 1-chome, Itabashi-ku, Tokyo 173-8515*
**Corresponding author. E-mail: smsatis@ipc.shizuoka.ac.jp*

(Received March 3, 2006; Accepted June 30, 2006)

Abstract: We report here the geology of Byôbu Rock and Gobanme Rock outcrops hitherto unmapped in the Prince Olav Coast, East Antarctica. Both these outcrops expose high-grade metamorphic and igneous rocks. The metamorphic rock units comprise mainly of gneisses migmatized to variable extent and amphibolites, whereas igneous rocks comprise of granites and pegmatites. Preliminary structural data obtained from the outcrops identified the regional, steep to moderately dipping foliation trend in the WNW-ESE at Byôbu Rock, whereas they trend in the NW-SE direction at Gobanme Rock. Two generations of folding were identified, an earlier tight isoclinal intrafolial folds and a late regional open fold. The three deformational events identified are comparable and consistent with those reported in the neighboring outcrops in the Prince Olav Coast. Metamorphic *P-T* conditions estimated based on various geothermobarometries indicate that the rocks have experienced granulite grade conditions during peak metamorphism (770–880℃ and 6–9 kbar). The finding of orthopyroxene at Byôbu Rock in this study extends the orthopyroxene-in isograd in the progressive metamorphic zone in the Lützow-Holm Complex further eastward beyond Tenmondai Rock. Inclusions of kyanite within garnet in metapelitic rocks suggest a clockwise *P-T* path, consistent with the *P-T* paths suggested for the Lützow-Holm Complex. Preliminary bulk rock geochemical investigations indicate that granitic rocks and quartzo-feldspathic gneiss mostly belong to volcanic arc granite suite, though their origin remains indistinct. Electron microprobe dating of monazites from representative rocks gave Pan-African ages (557±33 Ma), consistent with the regional metamorphic ages reported earlier. Thus, based on the similarities on structural, petrological, geochemical and geochronological data, the Byôbu Rock and Gobanme Rock are considered to be integral part of the Pan-African Lützow-Holm Complex with analogous geological history.

key words: Byôbu Rock, Gobanme Rock, Lützow-Holm Complex, metamorphic *P-T* evolution, monazite chemical ages

1. Introduction

Dronning Maud Land in East Antarctica forms an important geological unit in the

East Gondwana ensemble (Shiraishi *et al.,* 1994, 2003; Yoshida, 1995; Lawyer *et al.,* 1998). Geological field relations and metamorphic evolution of the exposures in this region are of general interest for East Gondwana correlation studies. Moreover, the high-grade metamorphic rocks exposed in the Dronning Maud Land can enlighten our basic understanding of the geodynamic evolution of the continental crust. Japanese Antarctic Research Expedition (JARE), over the past several decades, has been carrying out meticulous geologic field mapping along the Lützow-Holm Bay and Prince Olav Coast, within the eastern Dronning Maud Land (Fig. 1a). During the 46th JARE geological field expedition, we carried out a preliminary geologic mapping of two

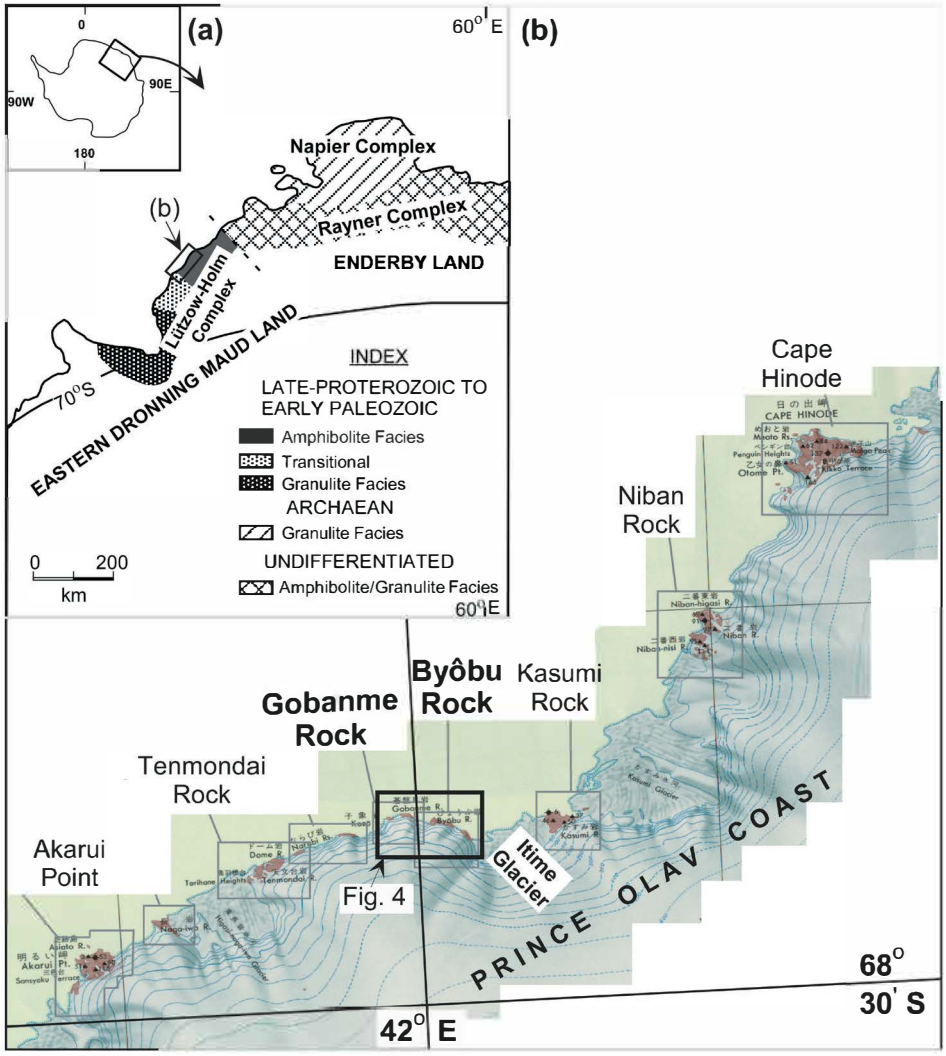

Fig. 1. (a) Geological outline of Dronning Maud Land. Progressive metamorphism observed in the Lützow-Holm Complex is after Hiroi et al. (1987). (b) Geographical distribution of Byôbu Rock and Gobanme Rock outcrops along the Prince Olav Coast.

hitherto unmapped outcrops of Byôbu Rock (BR) and Gobanme Rock (GR) situated in the Prince Olav Coast. BR and GR outcrops, situated between Tenmondai Rock in the west and Kasumi Rock in the east (Fig. 1b), are critical in many aspects of Prince Olav Coast geology, such as defining the metamorphic facies boundary, metamorphic *P-T* evolution and geochronology.

We present here, the general geology, preliminary whole rock geochemistry and metamorphic *P-T* estimates of the rock units exposed in the BR and GR outcrops. We also present monazite electron microprobe ages from three representative rock samples. Based on these results, we compare the geology of BR and GR with the general geology of the Prince Olav Coast.

2. General geology of Lützow-Holm Complex

The Lützow-Holm Complex comprises a major lithotectonic unit in the eastern Dronning Maud Land, situated between the Proterozoic Rayner Complex in the east and the central Dronning Maud Land in the west (Fig. 1a). This complex exposes a unique deep crustal section of granulite facies to amphibolite facies rocks of dominantly metasedimentary origin possibly formed during Paleo- to Neo-Proterozoic age. Several earlier studies have reviewed the geology of this metamorphic complex (Hiroi *et al.*, 1983, 1986, 1987; Shiraishi *et al.*, 1994, 2003). In general, there are two major phases of deformation, identified throughout the Lützow-Holm Bay region (Shiraishi *et al.,* 1983). Recent studies have further revealed the presence of an earlier deformation phase, thus suggesting three major deformation events for the region (Ikeda and Kawakami, 2004 and references therein).

Progressive metamorphism has been attributed to the Lützow-Holm Complex (Fig. 1a), with an increase in metamorphic grade from amphibolite facies in the north-east to granulite facies in the south-west region, the thermal maximum being reported from Rundvågshetta (Hiroi *et al.,* 1983). Peak metamorphic condition in the Lützow-Holm Bay is supposed to have reached up to about 1000°C at about 11 kbar in Rundvågshetta and nearby areas (Motoyoshi and Ishikawa, 1997; Fraser *et al.,* 2000; Yoshimura *et al.,* 2004). The presence of inclusions of kyanite, staurolite and sapphirine within garnet porphyroblasts suggests a clockwise *P-T* evolutionary history (Hiroi *et al.,* 1983; Motoyoshi *et al.*, 1989; Motoyoshi and Ishikawa, 1997).

Considerable attention has been paid to this terrain, in the last couple of decades, to decode the geochronologic history and its relevance to the Gondwana tectonics. For example, based on a detail SHRIMP analysis of zircons from different outcrops in the region, Shiraishi *et al.* (1994, 2003) suggested that this terrain was tectonothermally active during the Cambrian period. This is in concurrence with the general view that Pan-African tectonothermal event is the most prominent event in the eastern Dronning Maud Land, as is the case in many terrains of East Gondwana. Fraser *et al.* (2000) in an extensive geochronological study deciphered the *P-T-t* evolution of the high-temperature metamorphic rocks from Rundvågshetta. They put forward a model that involve a steep decompression in a short span of 7 My starting at about 520 Ma and thereafter cooling for about 13 My. This was followed by a slow thermal equilibration of the crust until about 420 Ma followed by a normal uplift.

3. General geology of Byôbu Rock and Gobanme Rock

BR and GR crops out between Tenmondai Rock in the west and Kasumi Rock in the east. Itime Glacier separates the Kasumi Rock and Byôbu Rock (Fig. 1b). The 42°E longitude and 68°22′S latitude passes through the Byôbu Rock outcrop. Gobanme Rock is about 2 km west of Byôbu Rock in the same latitude. Although both the exposures in this coastal stretch are small and narrow, a variety of rock units are exposed here, because the outcrops are at high angles to the generally steeply dipping strike of the rock units. Geological survey and sampling in these two outcrops were carried out for a day each in each outcrop.

Both BR and GR outcrops expose basement metamorphic rocks and igneous rocks. Although topography of these exposures consists of gentle slopes, coast lines have steep inaccessible cliffs. Aerial photographs, taken from the expedition helicopter, helped in extending the information gathered during field survey. Aerial photograph of the BR shows clearly the layered structure of the rock units in the area (Fig. 2a). Apart from the identification of major rock units based on surface features and weathering patterns, regional structural features of an antiform and a synform were delineated (Fig. 2b, c). The vertical cliff in the NW coast of BR display characteristic mesoscopic fold structures in the hinge of the regional antiform (Fig. 2c). The aerial photograph of GR also shows the distribution of major rock units and the general trend of the well-layered structure (Fig. 3).

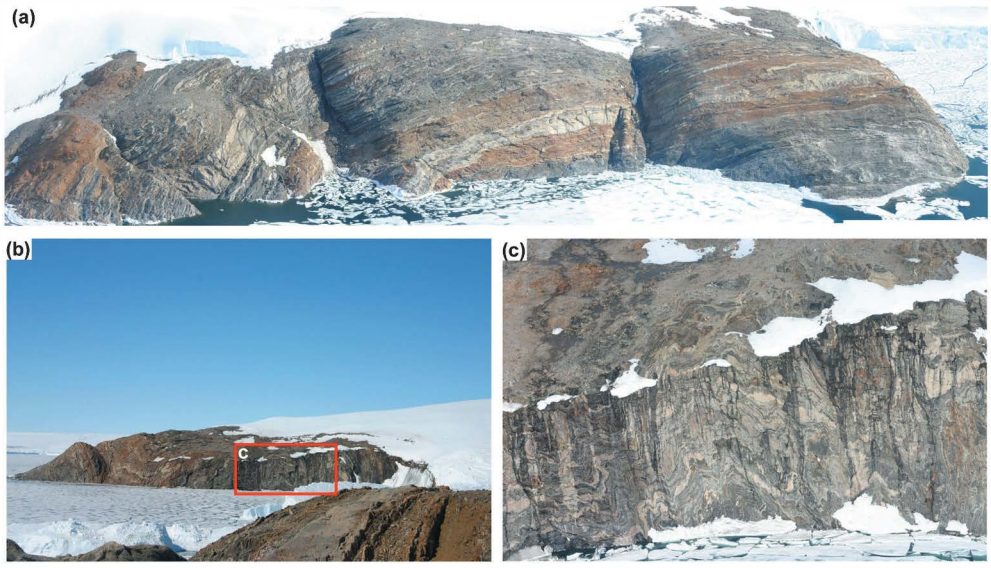

Fig. 2. Areal photograph of Byôbu Rock exposure showing the regional geological structure. (a) Photograph taken from the expedition helicopter facing towards WSW direction. (b) Byôbu Rock exposure as seen from Gobanme Rock. Photograph facing NNE direction. (c) Areal photograph of the coastal cliff in the Gobanme Rock exposure, showing intense folded structures. Cliff facing NNE direction.

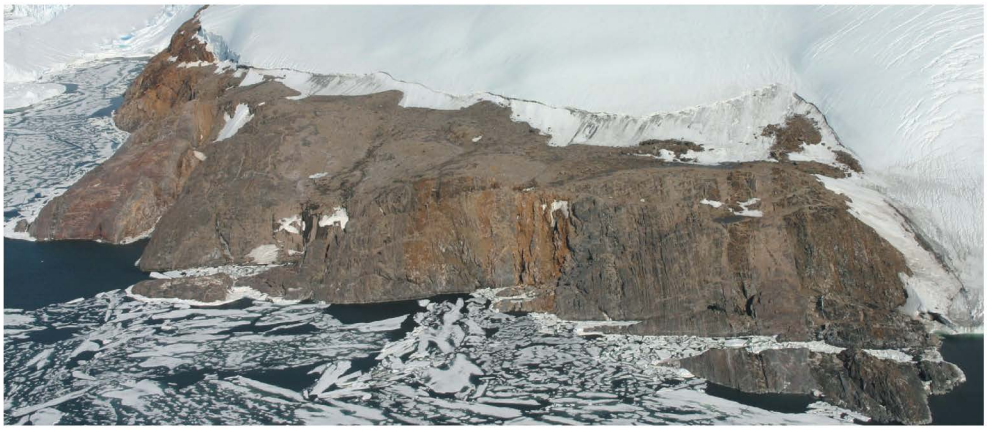

Fig. 3. Areal photograph of Gobanme Rock exposure showing the regional geological structure. Photograph taken from the expedition helicopter facing towards WSW direction.

Compiling the data obtained from the field and extending the information with the help of aerial photographs a geological map of BR and GR was prepared (Fig. 4).

4. Structural geology

4.1. Structural elements in the Byôbu Rock

The basement metamorphic rocks show well-defined layered structure that display a regional gneissic foliation, which trend between N75°W and N84°W (Fig. 4) with steep dips (55–72°S). Apart from the regional layering, this general trend is also visible by the thin, but mapable layers of amphibolites and granitic veins. Based on the aerial photographs and field data an antiform and a synform trending NW-SE direction was identified (Figs. 2b, 2c, 4). These regional folds have near vertical axial planes. Mesoscopic structures observed at BR include boudinage structures within the gneisses (Fig. 5a). In this northwestern part of BR, a rootless tight recumbent fold was observed (Fig. 5b). An outcrop scale megascopic open fold is observed in an amphibolite layer within the gneisses (Fig. 5c). This fold has a near vertical axial plane trending toward N72°W with the axis plunging 50°S. Numerous mesoscopic ptygmatic folds comprising of leucocratic veins are observed in the gneisses along the limbs of this fold (Fig. 5d).

4.2. Structural elements in the Gobanme Rock

GR outcrop also comprises of well layered gneisses with alternating bands of amphibolites (Fig. 4). Although the trend of the foliation shows minor variations, generally the layering define a foliation that trends N50°W with steep dips greater than 70°S. Amphibolites, with varying thicknesses (Fig. 6a), occur as bands parallel to the gneissic layering. Granitic gneisses are intruded by decimeter scale granitic veins (Fig. 6b). In the central region, the gneisses are extensively migmatized that are stromatic type (Fig. 6c). Layer parallel intrusions of pink granite and pegmatites of varying

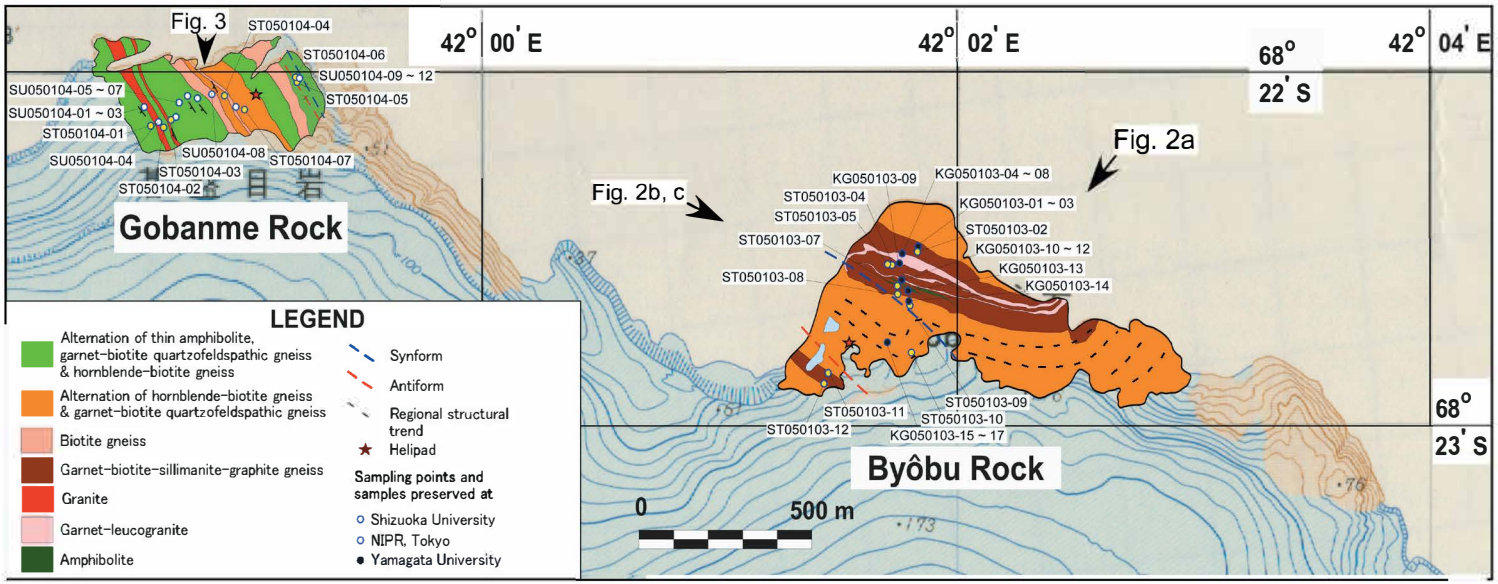

Fig. 4. Geological map of Byôbu Rock and Gobanme Rock outcrops. Solid and open circles represent sampling points.

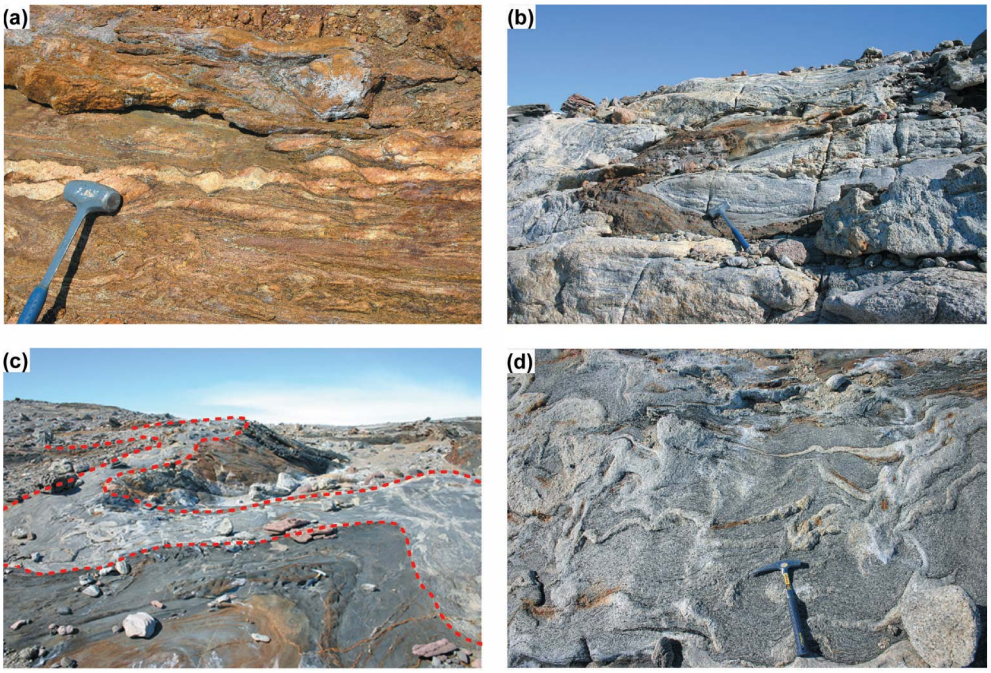

Fig. 5. Photographs showing examples of representative geologic structures observed in Byôbu Rock. (a) Boudinage quartzo-feldspathic layer within the pelitic gneiss near the contact with garnet leucogranite. (b) Rootless isooclinal near recumbent fold of mafic layer seen in the south-western region of BR. (c) Regional open folding seen in amphibolite and hornblende-biotite gnesiss in the central region of BR. (d) Folded leucocratic veins within migmatized hornblende-biotite gneiss.

thickness, up to a meter, are commonly observed in this outcrop (Fig. 6d).

Mesoscopic folds similar to those seen in BR are found in the western region of the Gobanme Rock (Fig. 6e). Here, a 2-m thick amphibolite layer is folded with the axial plane trending N60°W and the fold axis plunge towards 45°S. Several tight intrafolial folds were also observed within the amphibolite layers (Fig. 6f). These folds have near vertical axial plane trending N60°W with a plunge of 40–50°S and are considered to be synchronous. Earlier generation of granitic melt segregation are found along the fold hinges (Fig. 6g). Competent amphibolite layers and surrounding hornblende-gneiss preserve mesoscopic folds (Fig. 6h).

4.3. Deformation events

Although the collected structural data were limited, it is possible to tentatively assign the timing of deformation events observed in the BR and GR outcrops, because of the consistency in the general trend of the gneissosity as well as the recurrence of similar fold types in several exposures. The regional gneissic foliation and the trend defined by the layering are assigned as the major phase of the deformation event (D_m). Tight isoclinal folding (F_1) preserved in the competent amphibolite layers are considered here as a deformation event prior to the gneissic foliation (D_{m-1}). The regional open

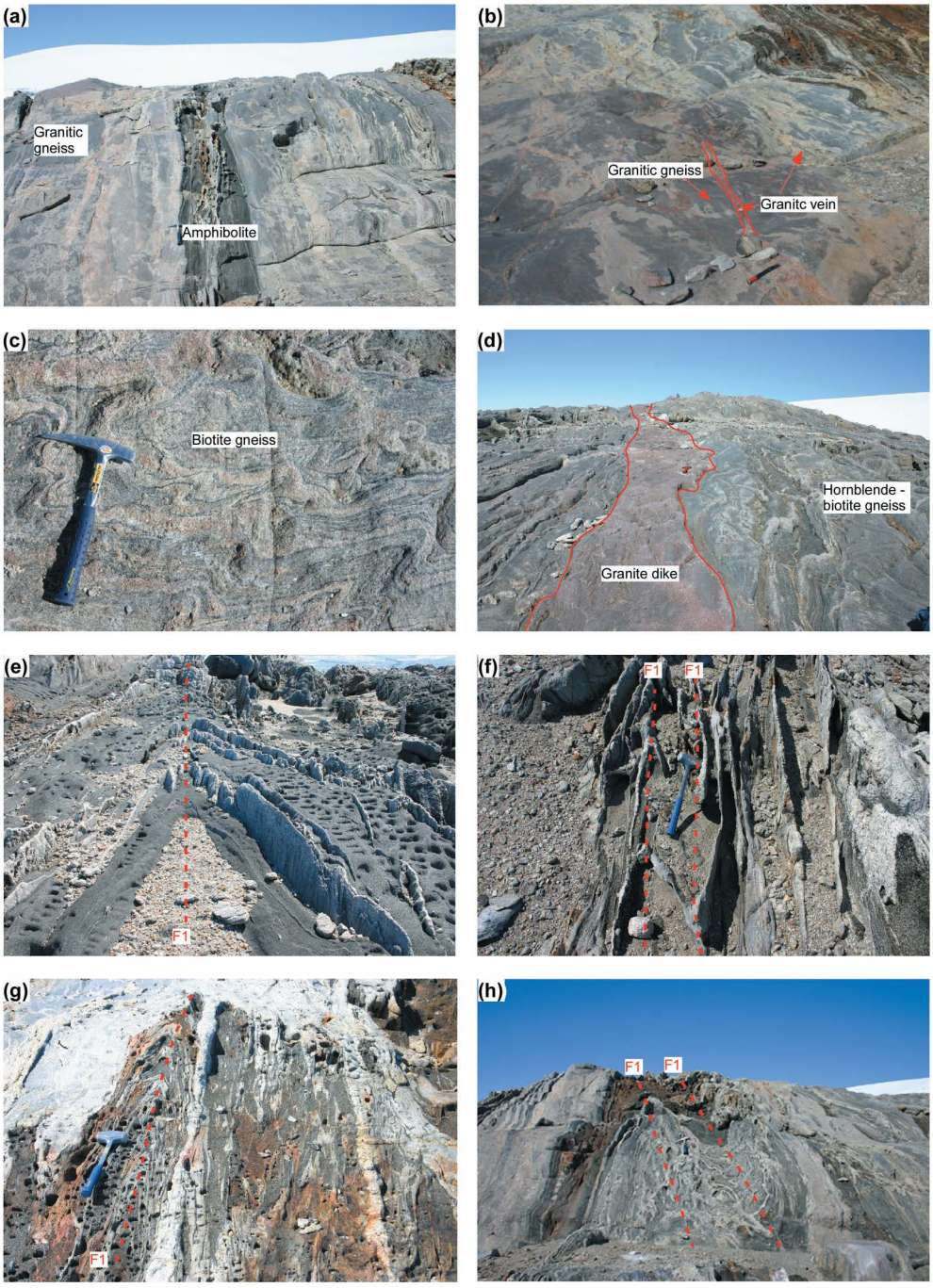
(a)
Granitic gneiss
Amphibolite
(b)
Granitic gneiss
Granitc vein
(c)
Biotite gneiss
(d)
Hornblende - biotite gneiss
Granite dike
(e)
F1
(f)
F1
F1
(g)
F1
(h)
F1
F1

Fig. 6.

antiform and synform (F_2) resulted from the latest phase of deformation in this region (D_{m+1}).

5. Lithologic units

The BR and GR are underlain by high-grade metamorphic rocks and syn-tectonic intrusive rocks. The basement metamorphic rocks comprise of gneisses, migmatites and amphibolites. Based on field observations and petrography we classified them into eight lithologic units (Table 1). Petrography of thin sections, prepared from the samples collected from the BR and GR outcrops, revealed the constituent mineral assemblages of the different rock units in the region (Table 1). Mineral abbreviations are after Kretz (1983).

In the BR exposure, garnet-biotite quartzo-feldspathic gneiss, hornblende-biotite gneiss and garnet-biotite-sillimanite-graphite gneiss predominate (Fig. 4). Thin layers of garnet-leucogranite and amphibolite occur within the pelitic gneiss. Gneissic rock units are subjected to anatexis to variable extent. Garnet-biotite quartzo-feldspathic gneiss is the prominent rock type here. Amphibolite layers are exposed in the northern area, where as hornblende-biotite-gneiss is more common in the southern region.

Compared with the BR exposure, amphibolites and granitic rocks predominate in the GR exposure (Fig. 4). Alternation of garnet-biotite quartzo-feldspathic gneiss and

Table 1. Lithologic units and mineral assemblages observed in BR and GR.

	Major mineral assembalges	Accessory minerals
Major rock units		
1) Garnet-biotite quartzo-feldspathic gneiss	Grt+Bt+Kfs+Qtz+Pl	Mt+Ilm+Ap+Zrc+Mnz±Gr
2) Hornblende-biotite gneiss	Hbl+Bt+Pl+Qtz±Grt	Mt+Ilm+Ap
3) Biotite gneiss	Bt+Kfs+Qtz+Pl±Grt	Mt+Ilm+Ap+Zrc+Mnz
4) Amphibolites	Hbl+Pl+Qtz±Grt±Bt±Opx±Cpx	Mt+Ap+Ttn
5) Garnet-sillimanite-graphite gneiss	Grt+Bt+Sil+Kfs+Qtz+Pl±Ky	Gr+Ilm+Ap+Zrc+Mnz
7) Garnet-leucogranite	Kfs+Qtz+Gt+Bt	Ilm +Zrc+Mnz
8) Granitic rocks and pegmatites	Kfs+Qtz+Pl+Bt	Mt+Ilm+Ap+Zrc+Mnz
Minor rock units		
1) Garnet-orthopyroxne granulite	Grt+Opx+Pl+Kfs+Bt+Qtz	Ilm+Rt+Zrc+Mnz
2) Calc-silicate rock	Pl+Cpx+Ttn+Cal	Ap

Fig. 6 (opposite). Photographs showing examples of macroscopic structures observed in Gobanme Rock outcrop. (a) Thin layer of amphibolite within the granitic gneiss in the western region of GR. (b) Granitic veins criss crossing the granitic gneiss in the western region of GR. (c) Highly folded migmatized biotite gneiss in the central region of GR. (d) Layer parallel intrusion of granitic dike in to granitic gneiss in the eastern region of GR. (e) Isoclinal tight fold shown by an amphibolite layer in the eastern region. (f) Numerous tight rootless isoclinal folds with vertical axial planes can be identified within the amphibolite layers. (g) Tightly folded amphibolites are intruded by granitc veins. (h) Meter scale folded layers are intruded by granitic gneiss in the eastern region of GR.

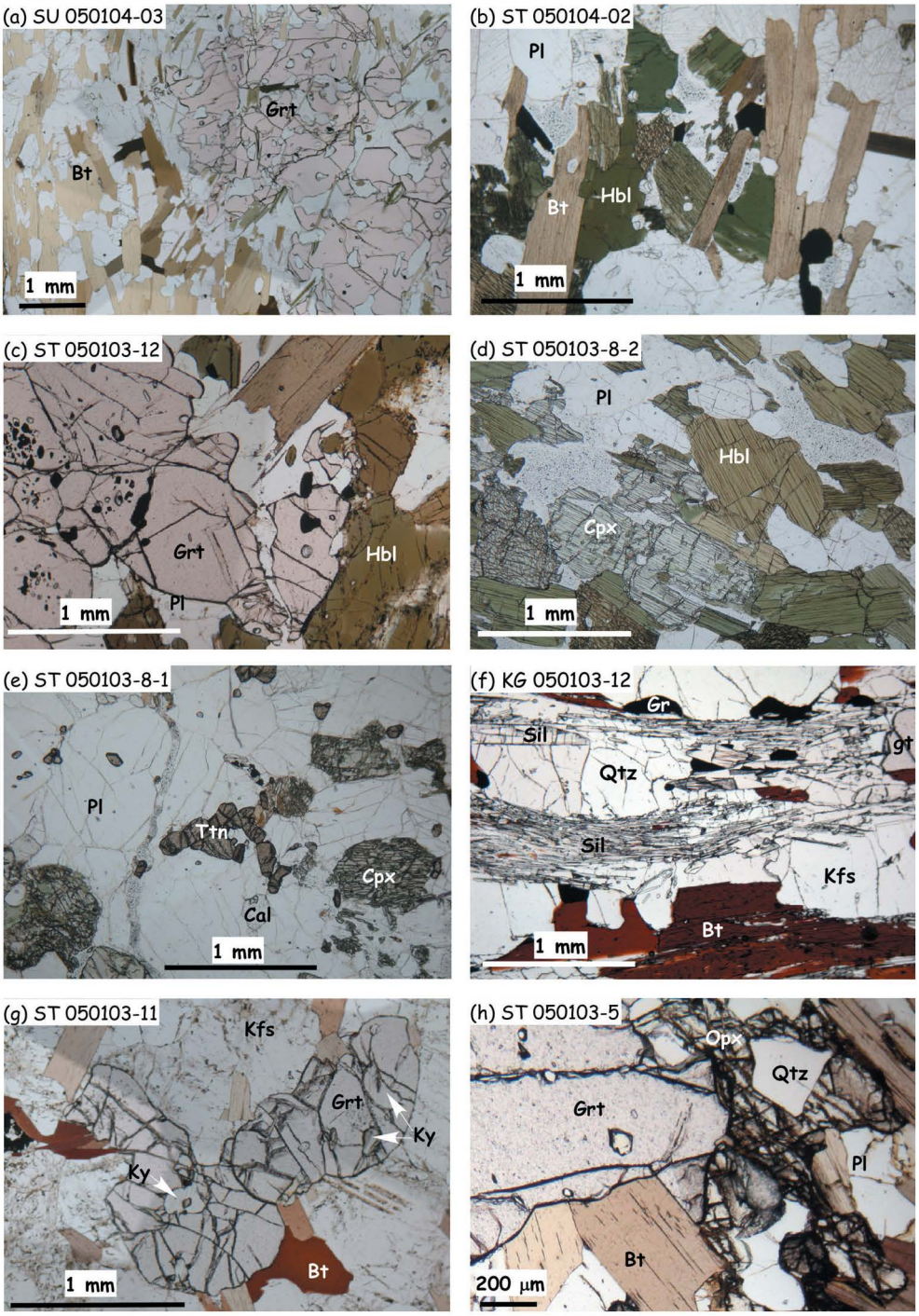
(a) SU 050104-03
Grt
Bt
1 mm
(b) ST 050104-02
Pl
Bt
Hbl
1 mm
(c) ST 050103-12
Grt
Hbl
Pl
1 mm
(d) ST 050103-8-2
Pl
Hbl
Cpx
1 mm
(e) ST 050103-8-1
Pl
Ttn
Cpx
Cal
1 mm
(f) KG 050103-12
Gr
Sil
Qtz
Sil
Kfs
Bt
1 mm
(g) ST 050103-11
Kfs
Grt
Ky
Ky
Bt
1 mm
(h) ST 050103-5
Opx
Qtz
Grt
Pl
Bt
200 µm

Fig. 7.

hornblende-biotite gneiss, observed in subordinate amounts in the central region, are migmatized. Layers of garnet-leucogranite are also observed in the eastern part of this outcrop. Layer parallel intrusion of pink granitic rocks and pegmatites are commonly observed in close association with amphibolites.

5.1. Garnet-biotite quartzo-feldspathic gneiss

This is the most widespread rock unit in the BR and less predominant in the GR. Layers have varying thickness, from few decimeters to more than ten meters, and are interlayered with amphibolites and hornblende-biotite gneiss. Typically, this rock unit comprises of alternating garnet＋biotite dominant layer and quartz＋feldspar dominant layers of varying thickness. Garnet porphyroblasts up to few centimeters in diameter are observed in some layers (Fig. 7a), commonly surrounded by biotite which defines the general foliation of the rock unit. In the quartzo-feldspathic layer, K-feldspars are coarse grained and mostly comprises of perthite, which are either microperthite or string perthite. Microcline is also observed in some samples. Plagioclase feldspars occur in minor amounts only. Accessory mineral phases include ilmenite, apatite, graphite, zircon and monazite.

5.2. Hornblende-biotite gneiss

Hornblende-biotite gneiss forms the second most abundant rock unit in the region. This rock type is commonly migmatized to variable extent. The mineral assemblage comprises of hornblende＋biotite＋plagioclase±garnet＋quartz with accessory amounts of titanite, apatite, and oxide phases. Hornblende and biotite are aligned to define the foliation (Fig. 7b). Inclusion of clinopyroxene or orthopyroxene within amphibole is not uncommon.

5.3. Biotite gneiss

Biotite gneiss is common in central region of the Gobanme Rock. They are characteristically well-layered, consisting of alternations of biotite-rich and quartzo-feldspathic layers. Mineralogically these rocks are simple comprising of quartz＋feldspar＋biotite±garnet. This rock unit is also subjected to varying degrees of anatexis.

5.4. Amphibolites

Amphibolite layers, commonly found in BR and GR, are massive in appearance. The northern region of the GR predominantly comprises of amphibolite layers. The thickness of the layers reaches up to few meters. Mineralogically, the amphibolites comprise mostly of hornblende and plagioclase, with subordinate amounts of biotite and

Fig. 7 (opposite). Representative photomicrographs of mineral assemblages observed in Byôbu Rock and Gabanme Rock. (a) Garnet porphyroblast in garnet-biotite-quartzo-feldspathic gneiss from Gobanme Rock. (b) Hornblende-biotite gneiss from Gobanme Rock. (c) Garnet-bearing amphibolite from Byôbu Rock. (d) Clinopyroxene relict in amphibolite from Byôbu Rock. (e) Calc-silicate rock showing clinopyroxene＋plagioclase＋titanite＋calcite assemblage. (f) Garnet-sillimanite-graphite-bearing gneiss from Byôbu Rock. (g) Kyanite inclusions within garnet in pelitic gneiss from Byôbu Rock. (h) Garnet-orthopyroxene-bearing granulite assemblage from Byôbu Rock. All photomicrographs are in plane polarized light.

quartz. Some amphibolite layers have garnet (Fig. 7c), whereas orthopyroxene and clinopyroxene occur as relicts, partially retrogressed to amphibole (Fig 7d). Oxide phases such as, ilmenite, rutile and magnetite are commonly found in amphibolites.

A thin (~10 cm) lens of calc-silicate rock was observed within the amphibolite layer at BR. This lens comprises of mostly clinopyroxene and plagioclase, with the core portions having abundant titanite (Fig. 7e). Quartz and calcite occur in accessory amounts.

5.5. Garnet-biotite-sillimanite-graphite gneiss

A thick layer of pelitic gneiss was observed in the northern part of BR. In other areas this rock unit occurs as thin discontinuous layers within the garnet-biotite quartzo-feldspathic gneiss unit. Characteristically, this unit, show reddish brown weathering surface, which can be easily identified in the aerial photographs (Fig. 2a). Gneissic banding is composed of garnet+biotite+sillimanite-rich domains and quartzo-feldspathic domains. Graphite is ubiquitously present in this unit. Gneissic foliation is defined by the arrangement of biotite, sillimanite and graphite (Fig. 7f). A mineral assemblage of garnet+sillimanite+biotite+graphite+quartz+K-feldspar+plagioclase +ilmenite is commonly found. Kyanite inclusions in garnet were observed in a thin layer, in which sillimanite is observed in the matrix (Fig. 7g). Usually garnet porphyroblasts (up to few cms) contain numerous mineral inclusions of quartz, feldspars, biotite, ilmenite and rutile. Biotite commonly occurs as aligned blades in the matrix. Sillimanite is also aligned, but occurs as aggregate surrounding garnet. K-feldspar commonly shows string-perthite structure, whereas plagioclase is present in subordinate amounts. Accessory phases include ilmenite, zircon, monazite and apatite.

5.6. Garnet-orthopyroxene granulite

A rare occurrence of garnet-orthopyroxene granulite was observed within the pelitic layer at BR. This lens shaped occurrence has a thickness of about 30 cm and comprise of garnet, biotite, orthopyroxene, plagioclase, K-feldspar and quartz (Fig. 7h). Garnet occurs as porphyroblasts up to few cms in diameter and contains numerous felsic mineral inclusions. The finding of orthopyroxene is significant because this can be considered as the easternmost occurrence in the metamorphic sequence of LHC.

5.7. Garnet-leucogranite

Several garnet-bearing leucogranitic layers of varying thickness occur in this region. The dominant minerals in this layer comprises of garnet+K-feldspar+quartz with subordinate amounts of biotite and muscovite. K-feldspars are mostly microperthite. Plagioclase occurs in subordinate amounts. Garnet is found as rounded grains which are larger in size than other constituent minerals and characteristically contain mineral inclusions of quartz and feldspars. Myrmekitic texture is commonly found. Apatite and zircon occur as accessory phases.

5.8. Granitic rocks and pegmatites

On the basis of field occurrence, granitic rocks in GR can be classified into meter-scale host granitic gneiss and decimeter-scale granitic veins. The granitic gneisses are

exposed as meter-scale layers in the eastern and western regions of GR, within which the granitic vein occur (Fig. 6b). Modal compositions indicate that the granitic gneiss shows typical mineralogy of granite, whereas the granitic vein has a mineralogy that varies from granite to granodiorite.

Granitic veins are composed of massive and coarse-grained minerals (up to 6 mm in diameter), which are bounded by relatively sharp contact with host granitic gneiss. The constituent minerals of the granitic veins are quartz (29–52% in modal composition) and plagioclase (40–41%) with or without K-feldspar (<30%) and biotite (<8 %), with zircon, actinolite, apatite and opaque minerals as accessory minerals. On the basis of Streckeisen's (1976) discrimination diagram, they range from tonalite through granodiorite to granite (Fig. 8a). Quartz, K-feldspar and plagioclase are euhedral to subhedral with grain-size up to 6 mm in diameter. Biotite is euhedral with grain-size between 0.5 to 2 mm in diameter.

On the other hand, granitic gneiss is composed of medium-grained minerals (up to 1 mm) with foliations. The direction of the foliation is consistent with those of the surrounding metamorphic rocks. The constituent minerals of the granitic gneiss are quartz (33–40%), K-feldspar (18–22%), plagioclase (32–40%) and biotite (6–9%), with garnet, zircon and opaque minerals as accessory minerals. On the basis of Streckeisen's (1976) discrimination diagram, they are predominantly granite (Fig. 8a). Quartz, K-feldspar and plagioclase are subhedral to anhedral with grain-size between 0.5 to 1 mm in diameter. Biotite is euhedral with grain-size *ca.* 0.5 mm in diameter, which are aligned to form the foliation of the granitic gneiss.

Intrusive dikes of pink granites and pegmatites are observed in both outcrops. The thickness of these dikes varies from decimeters to few meters. Most of the intrusions are parallel to the layering of the gneisses and amphibolites, however show irregular contact with the host gneiss (Fig. 6d). Intrusive field relations suggest a temporal gap between the last major deformation event and granitic intrusions. Mineralogically, these are typically of granitic composition with microcline and quartz as dominant minerals with subordinate amounts of biotite, muscovite, sphene, apatite and zircon.

6. Whole rock geochemistry

Whole-rock compositions of major and some trace elements of the metamorphic rocks and the granitic rocks from BR and GR were determined using a Rigaku X-ray fluorescence spectrometer (XRF) at the National Institute of Polar Research (NIPR). Representative whole-rock compositions are listed in Table 2, where contents of H_2O^+ and H_2O^- are included into the total weight percent of the major oxides.

Amphibolite and garnet-bearing amphibolite from Gobanme Rock have SiO_2 content between 45 and 57 wt%, and high concentration of Fe_2O_3 (8.5–17 wt%) relative to MgO (3.7–7.4 wt%), indicating basic to intermediate compositions. The SiO_2 contents of gneisses range from 64 to 74 wt% indicating intermediate to felsic compositions. On the other hand, those of the granitic rocks (garnet leuco-granite and granitic rocks) vary from 72 to 76 wt% indicating felsic composition. Values of alumna-saturation index (ASI: molar $Al_2O_3/(CaO+Na_2O+K_2O)$) indicate that the garnet-biotite quartzo-feldspathic gneiss and the granitic rocks have peraluminous signatures

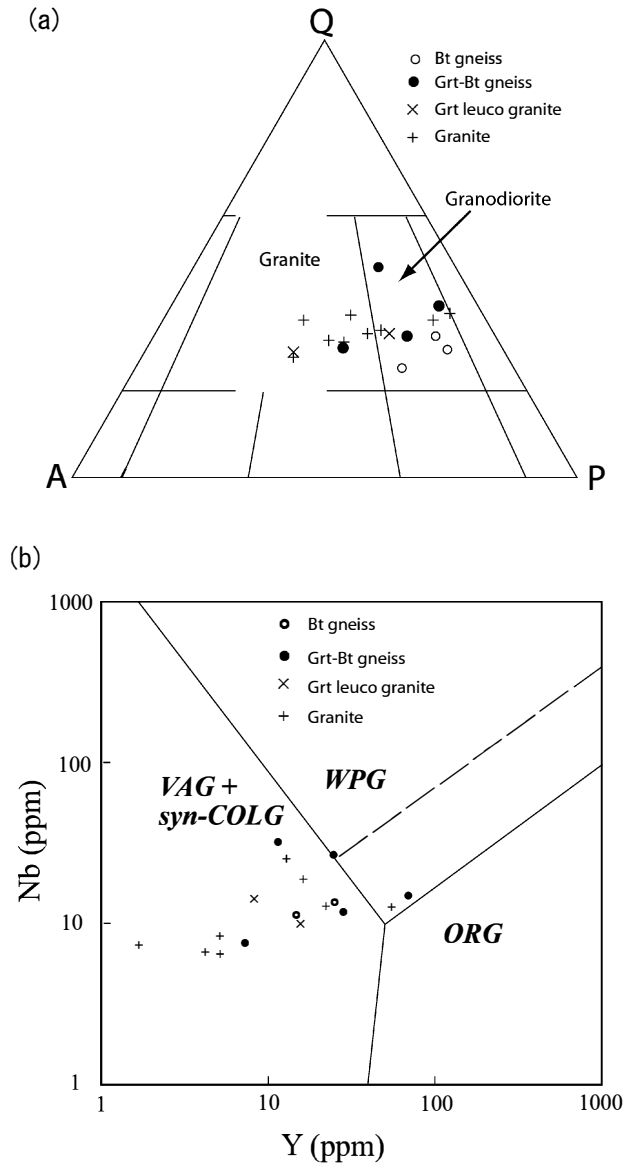

Fig. 8. (a) Modal composition of granitic rocks in terms of quartz (Q), alkali fieldspar (A) and plagioclase (P). Nomenclature from Streckeisen (1976) (b) Nb vs. Y discrimination diagram for granitoids in different tectonic setting (Pearce et al., 1984). Abbreviations: VAG, volcanic arc granite; WPG, within-plate granites; ORG, ocean ridge granite; syn-COLG, syn-collisional granite.

Table 2. Representative whole rock compositions.

Table 2 (continued).

(ASI $>$ 1.00). Figure 8b shows the discrimination diagram for granitoid rocks (Pearce *et al.,* 1984), in which the gneisses and the granitic rocks are predominantly plotted in the field of volcanic-arc granite. Only two samples (a granitic gneiss and garnet-biotite quartzo-feldspathic gneiss) are plotted in the field of with-in plate granite.

7. Mineral chemistry

Ten thin sections representing major metamorphic rock units (7 from BR and 3 from GR) were selected for mineral chemical analysis. Electron microprobe analyses of constituent minerals were carried out using a wave-length dispersive instrument (JEOL-JCXA733) at the Centre for Instrumental Analysis, Shizuoka University. Measurements were carried out at 15 kV accelerating voltage with a probe current of 1.2×10^{-8} A at a minimum ($\sim 1\,\mu$m) beam diameter. Natural and synthetic standards were used as reference materials and corrections were made according to Bence and Albee (1968) using α factors of Nakamura and Kushiro (1970).

7.1. Garnet

Garnet analyzed from all the rock types is essentially rich in almandine component with slight variations in pyrope and grossular contents (Table 3). Variations in garnet composition are shown in the ternary diagram (Fig 9). Garnet in garnet-biotite-sillimanite-graphite gneisses has a composition range of $Prp_{17\text{-}26}Alm_{68\text{-}78}Grs_{0\text{-}4}Sps_{2\text{-}3}$. Significant core to rim compositional variation is observed as shown in the compositional profile, especially in garnets in contact with other Fe-Mg phases (Fig. 10). Garnet in the garnet-biotite gneiss has a composition of $Prp_{16\text{-}22}Alm_{71\text{-}76}Grs_{0\text{-}8}Sps_{3\text{-}5}$ with less relevant compositional variation between core and rim. In garnet-bearing amphibolites, only nominal within grain compositional variation is observed in the range $Prp_{16\text{-}22}Alm_{54\text{-}62}Grs_{3\text{-}19}Sps_{3\text{-}10}$, although they have higher grossular content than the gneisses. Garnet in the garnet-orthopyroxene granulite has the highest pyrope content among all the analyzed samples. The compositional spread is in the range of $Prp_{21\text{-}33}Alm_{57\text{-}69}Grs_{1\text{-}14}Sps_{2}$. Core to rim variation is also observed (Fig. 10).

7.2. Biotite

Two compositional groups of biotite can be observed from the analyzed samples from BR and GR (Fig. 11), which basically correspond to the variations in the bulk rock chemistry. The X_{Mg} values of biotite in the gneisses lie around 0.5, whereas biotite in garnet-orthopyroxene granulite and one amphibolite sample has extremely high X_{Mg} values of around 0.63 (Table 4). There is large spread in Al content ranging from 2.4 to 3.3 apfu. All biotite have appreciably high titanium content, the lowest being found in amphibolites with 3.5 wt% and the highest of 5.7 wt% TiO_2 content was found in garnet-biotite-sillimanite-graphite gneiss.

7.3. Amphibole

Considerable compositional variation is observed in amphiboles, with X_{Mg} values varying in the range between 0.52 and 0.70 (Table 5). Based on the amphibole nomenclature by Leake *et al*. (1997), the BR and GR amphiboles from amphibolites

Table 3. Representative electron microprobe results of garnet.

Analysis No.	g 92	g 84	g 85	g 134	g 91	g 39	g 212	g 167	g 58	g 90
Sample No.	KG050103-03	KG050103-03	KG050103-11	KG050103-11	KG050103-12	KG050103-12	ST050103-5-1B	ST050103-5-1B	ST050103-5-1C	ST050103-5-1C
Locality	BR	BR	BR	BR	BR	BR	BR	BR	BR	BR
Rock type	Grt-Bt gneiss	Grt-Bt gneiss	Grt-Bt gneiss	Grt-Bt gneiss	Grt-Bt-Sil-Gr gneiss	Grt-Bt-Sil-Gr gneiss	Grt-Opx granulite	Grt-Opx granulite	Grt-Opx granulite	Grt-Opx granulite
Textural site	core	rim	core	rim	core	rim	core	rim	core	rim
SiO_2	36.79	37.38	37.41	37.19	35.85	37.44	38.11	38.11	38.69	38.86
TiO_2	0.32	0.33	0.31	0.33	0.30	0.31	0.30	0.34	0.29	0.30
Al_2O_3	19.95	20.64	20.77	21.07	21.14	20.30	20.45	20.75	21.78	21.41
Cr_2O_3	0.15	0.16	0.13	0.16	0.16	0.15	0.08	0.11	0.11	0.13
Fe_2O_3#	2.90	1.63	2.46	2.06	5.18	1.87	3.18	2.43	0.00	0.00
FeO	31.02	33.16	31.60	32.80	28.96	32.95	26.18	27.98	26.56	28.64
MnO	1.67	1.89	1.13	1.20	0.85	1.06	1.04	0.88	1.01	0.98
MgO	5.09	4.24	5.51	4.73	6.24	5.04	7.80	7.31	7.23	6.57
CaO	1.26	1.33	1.29	1.15	1.07	1.04	3.11	2.44	3.31	2.76
Na_2O	0.12	0.08	0.10	0.12	0.11	0.09	0.09	0.11	0.08	0.09
K_2O	0.11	0.10	0.11	0.10	0.11	0.09	0.10	0.11	0.10	0.10
Total	99.39	100.92	100.81	100.91	99.96	100.35	100.44	100.57	99.16	99.84
Cations on the basis of 12 oxygen				12	12	12	12	12	12	12
Si	2.957	2.971	2.951	2.944	2.847	2.980	2.962	2.967	3.015	3.031
Ti	0.020	0.020	0.019	0.020	0.018	0.018	0.018	0.020	0.017	0.018
Al	1.891	1.934	1.932	1.967	1.978	1.905	1.874	1.905	2.001	1.968
Cr	0.010	0.010	0.008	0.010	0.010	0.009	0.005	0.007	0.007	0.008
Fe^{3+} #	0.176	0.098	0.146	0.123	0.309	0.112	0.186	0.142	0.000	0.000
Fe^{2+}	2.085	2.204	2.085	2.172	1.923	2.193	1.702	1.822	1.731	1.868
Mn	0.114	0.127	0.075	0.081	0.057	0.072	0.068	0.058	0.067	0.065
Mg	0.610	0.502	0.647	0.558	0.738	0.598	0.903	0.848	0.840	0.764
Ca	0.109	0.113	0.109	0.098	0.091	0.089	0.259	0.204	0.276	0.231
Na	0.019	0.012	0.016	0.018	0.017	0.014	0.014	0.017	0.012	0.014
K	0.011	0.010	0.011	0.010	0.011	0.009	0.010	0.011	0.010	0.010
Total	8.000	8.000	8.000	8.000	8.000	8.000	8.000	8.000	7.975	7.975
X_{Mg}	0.23	0.19	0.24	0.20	0.28	0.21	0.35	0.32	0.33	0.29

calculated

vary from magnesiohastingsite and pargasite to edenite. TiO_2 contents vary from 1.7 to 2.2 wt%.

7.4. Pyroxene

Orthopyroxene was identified in two samples, an amphibolite and a granulite, both having similar chemical composition (Table 5). Orthopyroxene with X_{Mg} values of 0.53–0.54 occur in one amphibolite sample. The Al_2O_3 content is up to 1.5 wt%. Orthopyroxene in the garnet-orthopyroxene granulite have X_{Mg} values in the range between 0.55 and 0.62. The Al_2O_3 content are in the range between 1.8 and 2.2 wt%.

7.5. Feldspar

Plagioclase feldspars in gneisses are albite-rich in composition (Ab_{75-82}) (Table 6). However, those in amphibolites are anorthite-rich and show large spread in composition between An_{38} and An_{80}. Plagioclase in the garnet-orthopyroxene granulite has a composition in the range An_{28}–An_{34}. K-feldspars in gneisses and granitic rocks have low albite contents (Or_{95} Ab_5).

Table 3 (continued).

g 67	g 100	g 43	g 44	g 59	g 17	g 65	g 93	g 21	g 61
ST050103-11-1B	ST050103-11-1B	ST050103-12-2-2B	ST050103-12-2-2B	SU050104-02	SU050104-02	SU050104-03	SU050104-03	SU050104-08	SU050104-08
BR	BR	BR	BR	GR	GR	GR	GR	GR	GR
Grt-Bt-Sil-Gr gneiss	Grt-Bt-Sil-Gr gneiss	Amphibolite	Amphibolite	Amphibolite	Amphibolite	Amphibolite	Amphibolite	Amphibolite	Amphibolite
core	rim	core	rim	core	rim	core	rim	core	rim
37.52	37.24	37.96	37.89	37.94	37.86	38.23	37.98	37.35	37.73
0.37	0.32	0.34	0.33	0.34	0.34	0.32	0.32	0.33	0.33
21.11	21.31	21.50	21.46	19.81	20.05	19.07	20.50	21.32	21.37
0.19	0.18	0.15	0.14	0.16	0.16	0.17	0.16	0.12	0.20
0.00	0.00	0.08	0.34	3.08	2.03	2.31	2.30	2.77	1.73
33.74	32.75	26.29	26.37	24.40	26.60	25.67	26.71	23.72	26.77
0.96	0.85	1.39	1.52	2.39	3.33	2.52	4.02	1.47	1.80
4.03	4.65	4.88	4.91	4.51	4.47	5.20	4.25	6.06	5.17
0.94	1.44	6.68	6.45	7.92	5.47	6.14	5.17	6.55	5.34
0.10	0.09	0.10	0.08	0.08	0.07	0.08	0.09	0.06	0.10
0.12	0.10	0.09	0.10	0.09	0.10	0.09	0.10	0.09	0.10
99.08	98.93	99.47	99.59	100.72	100.47	99.78	101.59	99.84	100.64
12	12	12	12	12	12	12	12	12	12
3.014	2.987	2.987	2.982	2.978	2.991	3.028	2.974	2.921	2.951
0.022	0.019	0.020	0.020	0.020	0.020	0.019	0.019	0.019	0.019
1.999	2.015	1.995	1.991	1.833	1.867	1.781	1.893	1.966	1.971
0.012	0.011	0.009	0.009	0.010	0.010	0.011	0.010	0.007	0.012
0.000	0.000	0.005	0.020	0.182	0.121	0.137	0.135	0.163	0.102
2.267	2.197	1.731	1.736	1.602	1.758	1.700	1.749	1.552	1.751
0.065	0.058	0.093	0.101	0.159	0.223	0.169	0.266	0.097	0.119
0.483	0.556	0.572	0.576	0.528	0.526	0.613	0.496	0.706	0.602
0.081	0.124	0.563	0.544	0.666	0.463	0.521	0.434	0.549	0.448
0.016	0.014	0.015	0.012	0.013	0.011	0.012	0.013	0.009	0.015
0.012	0.010	0.009	0.010	0.009	0.010	0.009	0.010	0.009	0.010
7.972	7.992	8.000	8.000	8.000	8.000	8.000	8.000	8.000	8.000
0.18	0.20	0.25	0.25	0.25	0.23	0.27	0.22	0.31	0.26

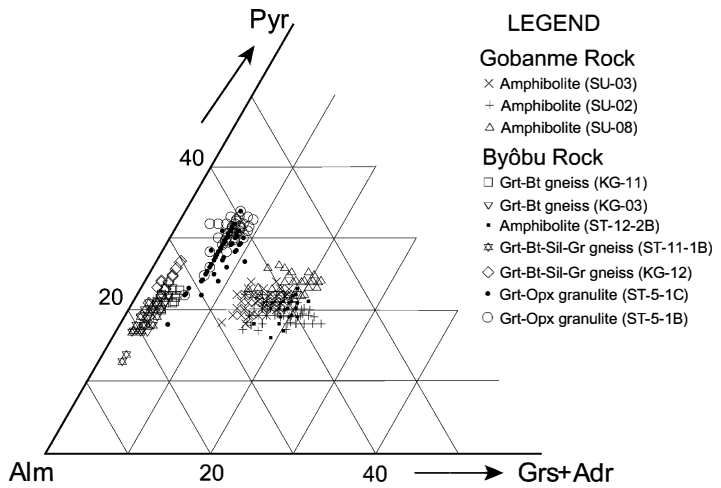

Fig. 9. Triplot showing garnet compositional variation observed in different rocks units. The domains representing the groups correspond to the specific bulk rock chemistry.

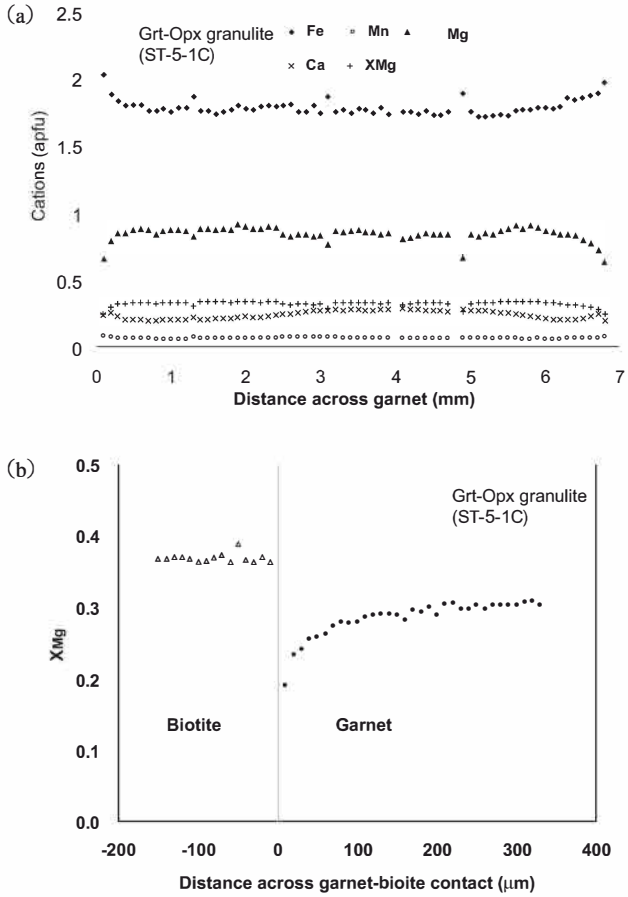

Fig. 10. (a) Compositional profile of garnet in garnet-orthopyroxene granulite. (b) Compositional profile across garnet-biotite contact in garnet-orthopyroxene granulite.

7.6. Accessory minerals

Opaque minerals are the most common accessory phases. They include ilmenite, magnetite, rutile and sulphide group minerals. Titanite and apatite are found in subordinate amounts in amphibolites, whereas graphite is common in garnet-biotite-sillimanite-graphite gneiss. Zircon and monazite are commonly observed in gneisses.

8. Metamorphic *P-T* conditions

Five samples from three lithologic units were selected for the estimation of pressure-temperature conditions. Conventional Fe-Mg cation exchange geothermometery based on garnet-biotite and garnet-orthopyroxene were applied. Net transfer equilibria based on the garnet-aluminosilicate-plagioclase-quartz (GASP) and garnet-orthopyroxene-plagioclase-quartz (GOPQ) were also utilized. *P-T* estimates obtained in the present study are summarized in Table 7.

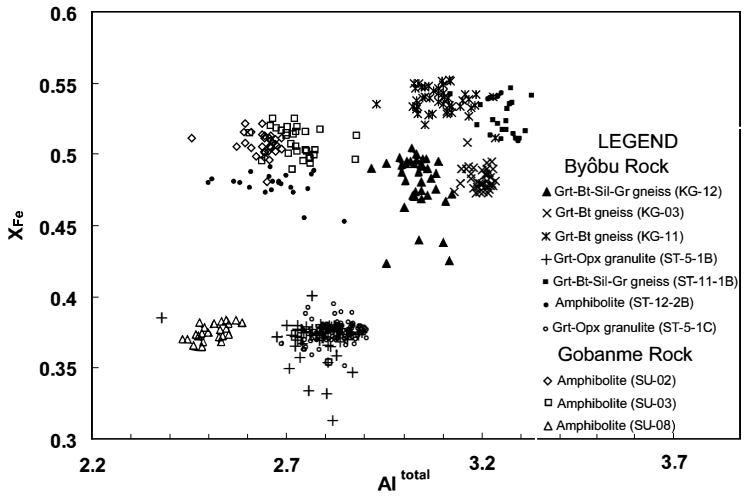

Fig. 11. Chemical variation observed in biotite from different rock units.

8.1. Garnet-biotite geothermometry

Garnet-biotite geothermometry, based on the Fe-Mg equilibria, is one among the most widely used method for determining the metamorphic temperature, because garnet and biotite are the most common minerals in the high-grade metamorphic rocks world wide. However, Fe and Mg in garnet and biotite are susceptible to compositional exchange during retrograde conditions. This diffusional retrograde Fe-Mg exchange is clearly visible in a compositional profile across a garnet in contact with biotite analyzed in this study (Fig. 10b). Furthermore, the presence of other elements, such as titanium in biotite, hinder in the accurate computation of temperature. Several earlier workers have discussed the limitations of garnet-biotite geothermometry, and the protocol we follow include selection of garnet core composition having the most Mg-rich domains and biotite core composition of grains surrounded by felsic minerals, absence of other Fe-Mg-bearing minerals and predominance of garnet to biotite in the rock (Spear 1991; Spear and Florence, 1992). Calibrations used in this study were based on Ganguly and Saxena (1984) and Dasgupta *et al.* (1991).

X_{Mg} values of garnet and co-exisiting biotite show consistent equilibrium conditions as evidenced by similar K_D values irrespective of variations in bulk rock chemistry (Fig. 12). Minor variations observed are relating to intra-granular chemical variation caused by the retrograde exchange. Core compositions of garnet and matrix biotite gave maximum temperature estimates of 770°C at 8 kbar (Table 7). Lower temperature estimates of up to 600°C were obtained form garnet-biotite pairs that sustained cation exchange during retrograde cooling.

8.2. Garnet-orthopyroxene geothermometry

Garnet-orthopyroxene Fe-Mg exchange thermometry of Sen and Bhattacharya (1984) and Lee and Ganguly (1988) were employed to estimate peak metamorphic temperature conditions in the garnet-orthopyroxene granulite sample. Garnet core

Table 4. Representative electron microprobe results of biotite.

Analysis No.	bi 58	bi 93	bi 100	bi 102	bi 85	bi 100	bi 41	bi 295
Sample No.	KG050103-03	KG050103-03	KG050103-11	KG050103-11	KG050103-12	KG050103-12	ST050103-5-1B	ST050103-5-1B
Locality	BR	BR	BR	BR	BR	BR	BR	BR
Rock type	Grt-Bt gneiss	Grt-Bt gneiss	Grt-Bt gneiss	Grt-Bt gneiss	Grt-Bt-Sil-Gr gneiss	Grt-Bt-Sil-Gr gneiss	Grt-Opx granulite	Grt-Opx granulite
Textural site	matrix	incl in grt	matrix	rim with grt	matrix	incl in grt	matrix	incl in grt
SiO_2	35.01	35.62	34.63	36.07	34.16	35.16	37.32	37.48
TiO_2	4.50	5.24	6.06	4.17	5.79	4.80	4.15	4.14
Al_2O_3	18.07	17.64	17.09	18.43	16.76	17.15	16.27	16.80
Cr_2O_3	0.19	0.17	0.12	0.12	0.20	0.22	0.11	0.11
FeO	17.65	15.55	19.35	18.49	18.26	16.75	14.88	12.93
MnO	0.21	0.17	0.19	0.18	0.15	0.15	0.15	0.14
MgO	10.42	13.15	8.96	9.90	10.43	11.97	14.47	15.94
CaO	0.15	0.18	0.13	0.15	0.17	0.16	0.14	0.14
Na_2O	0.16	0.50	0.16	0.13	0.20	0.22	0.52	0.53
K_2O	9.09	9.01	9.29	9.39	9.22	9.39	8.82	8.66
Total	95.46	97.26	95.98	97.05	95.36	95.98	96.84	96.88
Cations on the basis of 11 oxygen								
Si	2.646	2.617	2.633	2.684	2.607	2.640	2.733	2.714
Ti	0.256	0.290	0.346	0.233	0.332	0.271	0.229	0.225
Al	1.610	1.528	1.532	1.617	1.508	1.519	1.405	1.434
Cr	0.011	0.010	0.007	0.007	0.012	0.013	0.006	0.006
Fe^{2+}	1.115	0.955	1.230	1.151	1.166	1.052	0.911	0.783
Mn	0.013	0.011	0.012	0.012	0.010	0.009	0.009	0.009
Mg	1.173	1.439	1.015	1.098	1.187	1.339	1.579	1.720
Ca	0.012	0.014	0.011	0.012	0.014	0.013	0.011	0.011
Na	0.024	0.072	0.024	0.019	0.029	0.032	0.074	0.074
K	0.877	0.846	0.902	0.893	0.899	0.900	0.825	0.801
Total	7.738	7.783	7.714	7.726	7.764	7.789	7.782	7.778
X_{Mg}	0.51	0.60	0.45	0.49	0.50	0.56	0.63	0.69

compositions gave a temperature estimate in the range of 800–880°C at pressure conditions of 8 kbar, whereas the rim compositions gave temperature estimates in the range 730–760°C at same pressures. Temperature estimates corrected for retrograde exchange based on the convergence method of Pattison *et al.* (2003) gave considerably higher temperature up to 1000°C.

8.3. Garnet-aluminosilicate-plagioclase-quartz geobarometry

For aluminous metapelitic assemblages we estimated the pressure conditions during the peak metamorphism based on the net transfer reaction of anorthite and grossular + aluminosilicate + quartz. The calibrations of Newton and Haselton (1981) and Ganguly and Saxena (1984) were applied. Pressure estimates obtained for garnet core compositions range from 6.1 to 9.6 kbar at 800°C.

Table 4 (continued).

bi 114	bi 17	bi110	bi-1-19	bi-1-26	bi 171	bi 133	bi 72
ST050103-5-1C	ST050103-11-1B	ST050103-11-1B	SU050104-02	SU050104-02	SU050104-03	SU050104-03	SU050104-08
BR	BR	BR	GR	GR	GR	GR	GR
Grt-Opx granulite	Grt-Bt-Sil-Gr gneiss	Grt-Bt-Sil-Gr gneiss	Amphibolite	Amphibolite	Amphibolite	Amphibolite	Amphibolite
matrix	rim with grt	matrix	matrix-1	matrix-2	matrix core	incl in grt	matrix
37.20	35.02	35.33	35.28	35.20	35.95	36.84	36.59
4.37	5.27	5.45	4.84	4.78	3.97	1.21	4.67
16.61	18.16	18.04	14.33	14.87	15.38	15.90	14.30
0.11	0.19	0.19	0.12	0.15	0.18	0.11	0.21
14.51	16.96	17.75	20.34	20.39	20.54	14.29	15.43
0.17	0.15	0.18	0.25	0.29	0.29	0.17	0.17
13.28	8.86	8.50	11.05	11.16	10.84	14.67	14.62
0.28	0.22	0.15	0.15	0.14	0.14	0.18	0.15
0.48	0.18	0.22	0.18	0.20	0.17	0.17	0.34
8.28	9.51	9.62	9.22	9.13	9.15	8.91	9.08
95.30	94.53	95.44	95.77	96.30	96.62	95.24	95.57
2.754	2.669	2.677	2.709	2.686	2.727	2.758	2.741
0.243	0.302	0.311	0.280	0.274	0.226	0.068	0.263
1.450	1.632	1.612	1.297	1.337	1.375	1.404	1.262
0.006	0.011	0.011	0.007	0.009	0.011	0.006	0.013
0.898	1.081	1.125	1.306	1.301	1.303	0.895	0.966
0.011	0.010	0.012	0.016	0.019	0.019	0.011	0.011
1.465	1.007	0.960	1.265	1.269	1.226	1.637	1.632
0.022	0.018	0.012	0.013	0.012	0.012	0.014	0.012
0.069	0.027	0.032	0.026	0.029	0.026	0.025	0.049
0.783	0.926	0.931	0.905	0.889	0.887	0.852	0.869
7.701	7.683	7.682	7.824	7.826	7.810	7.828	7.818
0.62	0.48	0.46	0.49	0.49	0.48	0.65	0.63

8.4. Garnet-orthopyroxene-plagioclase-quartz geobarometry

This geobarometry is based on the net transfer exchange reaction between garnet + quartz and orthopyroxene + plagioclase. Calibrations based on Newton and Perkins (1982) and Bhattacharya *et al.* (1991) were employed. Garnet core compositions gave pressure conditions in the range from 6.6 to 9 kbar at 800°C, whereas rim compositions gave pressure condition of about 4–6.5 kbar at 600°C.

8.5. Summary of P-T estimates

Irrespective of the calibrations used or methodology, garnet core compositions in equilibrium with other Fe-Mg-Ca phases indicate a peak metamorphic temperature of around 770°C–880°C and pressure conditions of around 6–9 kbar (Fig. 13). Rim compositions which might have equilibrated during the retrograde conditions gave consistently lower *P-T* conditions than the peak metamorphic conditions. Temperature estimates of around 600°C at 4–5 kbar are considered to be best estimates for retrograde conditions at BR and GR.

Table 5. Representative mineral chemistry of orthopyroxene and amphibole.

Analysis No.	opx 148	opx 146	opx1-44	opx1-88	amph 22	amph 33	amph 1-55	amph 39	amph 44
Sample No.	ST050103-5-1B	ST050103-5-1B	ST050103-5-1C	ST050103-5-1C	ST050103-12-2-2B	ST050103-12-2-2B	SU050104-02	SU050104-08	SU050104-08
Locality	BR	BR	BR	BR	BR	BR	GR	GR	GR
Rock type	Grt-Opx granulite	Grt-Opx granulite	Grt-Opx granulite	Grt-Opx granulite	Amphibolite	Amphibolite	Amphibolite	Amphibolite	Amphibolite
Mineral/ Textural site	opx-core	opx-rim	opx-core	opx-rim	amph matrix	amph matrix	amph	amph core	amph rim
SiO_2	50.77	50.90	52.92	51.67	39.95	41.18	41.58	43.18	45.36
TiO_2	0.38	0.37	0.39	0.37	2.21	1.91	2.09	1.94	1.82
Al_2O_3	1.91	1.83	2.24	2.68	12.44	11.78	11.29	11.44	11.00
Cr_2O_3	0.15	0.10	0.10	0.12	0.13	0.14	0.15	0.20	0.19
Fe_2O_3#	2.44	3.25	0.00	0.00	0.32	2.86	5.92	5.86	2.72
FeO	24.15	24.00	25.09	25.16	15.70	13.30	13.85	9.55	11.40
MnO	0.40	0.40	0.42	0.37	0.31	0.33	0.58	0.39	0.32
MgO	19.90	20.05	19.34	17.89	8.77	9.71	9.35	12.19	12.46
CaO	0.31	0.30	0.40	0.52	11.58	11.42	11.14	10.64	11.38
Na_2O	0.07	0.08	0.09	0.11	1.67	1.31	1.56	1.55	1.53
K_2O	0.10	0.10	0.10	0.24	1.07	0.82	1.06	0.76	0.63
Total	100.58	101.38	101.09	99.13	94.15	94.77	98.57	97.70	98.80
Cations on the basis of (O)	6	6	6	6	23	23	23	23	23
Si	1.915	1.907	1.969	1.967	6.254	6.341	6.241	6.357	6.575
Ti	0.011	0.010	0.011	0.011	0.260	0.221	0.236	0.215	0.199
Al	0.085	0.081	0.098	0.120	2.296	2.138	1.997	1.985	1.880
Cr	0.004	0.003	0.003	0.004	0.016	0.017	0.018	0.024	0.022
Fe^{3+}#	0.069	0.092	0.000	0.000	0.038	0.332	0.668	0.649	0.297
Fe^{2+}	0.762	0.752	0.781	0.801	2.056	1.713	1.739	1.175	1.382
Mn	0.013	0.013	0.013	0.012	0.041	0.043	0.074	0.049	0.039
Mg	1.119	1.120	1.072	1.015	2.046	2.228	2.090	2.674	2.691
Ca	0.013	0.012	0.016	0.021	1.943	1.884	1.791	1.679	1.768
Na	0.005	0.006	0.006	0.008	0.507	0.391	0.453	0.443	0.431
K	0.005	0.005	0.005	0.012	0.214	0.161	0.204	0.143	0.116
Total	4.000	4.000	3.975	3.970	15.671	15.470	15.510	15.392	15.400
X_{Mg}	0.59	0.60	0.58	0.56	0.50	0.57	0.55	0.69	0.66

calculated

9. Geochronology

9.1. Analytical techniques

Quantitative chemical analyses on monazite were performed by means of a wavelength dispersive (WDS) electron microprobe analyzer (JEOL JXA-8800 equipped with five detectors) installed at the National Institute of Polar Research, Tokyo. The operating conditions were 15 kV accelerating voltage, 0.2 μA beam current and 2 μm beam diameter (Hokada *et al.*, 2004). In addition to UO_2, ThO_2 and PbO, other REE, SiO_2, CaO, P_2O_5 and ZrO_2 were also measured, and the intensity data were adjusted to $\phi\rho(Z)$ correction method. Among the analyses, those with higher than 0.02 wt% PbO were selected for further processing. Analytical results are given in Appendix 1.

Monazite grains were commonly detected in matrix and rarely as inclusions in garnet in the three representative samples analyzed from BR. Grain size varies from 5 to 200 μm. BSE images obtained for the monazite grains does not show zoning patterns or overgrowth textures. All monazite grains within the thin section were targeted and

several spots (3–10) measured within each grain (see Appendix 1).

9.2. Results

Sample KG 11 (KG05010311) is a garnet-biotite-sillimanite-graphite gneiss with porphyroblastic garnet of about 1 cm diameter. Seventeen monazite grains were analyzed, one of which was included in the garnet porphyroblast. All the other monazite grains occur in the matrix in close association with biotite (Figs. 14a, c). Apparent ages of single spots range from 663 Ma to 495 Ma and the sample has an average age of 563±32 Ma. There is no distinct age grouping between the core and the rim portions (Fig. 14b, d).

In the sample KG 03 (KG 05010303), which is a typical garnet-biotite quartzo-feldspathic gneiss, monazite grains occur in the matrix in association with biotite and feldspars. Eight monazite grains were analyzed which gave apparent ages in the range 615 Ma to 479 Ma. Average apparent age is 551±24 Ma. The lowest apparent age of 479 Ma is close to a fracture.

Sample ST 5-1B-2 (ST050103-5-1B-2) is a garnet-orthopyroxene granulite, where centimeter scale garnets occur as a porphyroblasts within a biotite+orthopyroxene-rich matrix. Less number of monazite grains could be detected in this rock. Five matrix monazite grains and one monazite inclusion in garnet were analyzed in this sample. The range of apparent ages is from 571 Ma to 481 Ma, having an average of 546±40 Ma. The age distribution does not show any distinct populations with respect to cores or rims or inclusions within garnet.

10. Discussion

10.1. Metamorphic conditions and P-T evolution

The estimated metamorphic *P-T* conditions from the rocks of BR and GR suggest granulite facies conditions. Incidentally, these outcrops lie east of Tenmondai Rock outcrop, where Hiroi *et al.* (1983) identified the first appearance of orthopyroxene in the metabasic rocks. The finding of orthopyroxene-bearing assemblages in BR suggests the re-location of the orthopyroxene-in isograd. This is further supported by the peak metamorphic *P-T* conditions estimated using various geothermobarometries. In addition, we could also observe field evidences for anatexis in the gneisses of BR and GR. Altogether, it can be concluded that the BR and GR outcrops have attained granulite facies conditions and subjected to partial melting. This peak metamorphic condition is comparatively higher by about 100 to 150°C to the earlier regional temperature estimates in the Prince Olav Coast (Hiroi *et al.,* 1983). We attribute this discrepancy to the calibrations used in earlier studies. If we consider the regional temperature variations in LHC, our temperature estimates are lower than the UHT conditions recently recognized from the Rundvågshetta and surrounding areas (Motoyoshi and Ishikawa, 1997; Yoshimura *et al.,* 2004). Furthermore, the eastward decrease in temperature conditions is consistent with the model of progressive metamorphism for the crustal section of LHC (Hiroi *et al.,* 1983).

The estimated retrograde metamorphic *P-T* conditions from the garnet-biotite quartzo-feldspathic rocks indicate that these rocks have recorded lower temperature of

Table 6. Representative mineral chemistry of feldspars.

Analysis No.	fsp 21	fsp 28	fsp 32	fsp 75	fsp 62	fsp 100	fsp 313	fsp 1-57
Sample No.	KG050103-03	KG050103-03	KG050103-11	KG050103-12	KG050103-12	ST050103-5-1B	ST050103-5-1B	ST050103-5-1C
Locality	BR	BR	BR	BR	BR	BR	BR	BR
Rock type	Grt-Bt gneiss	Grt-Bt gneiss	Grt-Bt gneiss	Grt-Bt-Sil-Gr gneiss	Grt-Bt-Sil-Gr gneiss	Grt-Opx granulite	Grt-Opx granulite	Grt-Opx granulite
Mineral/ Textural site	Pl-core	Pl-rim	Kfs-core	Pl-core	Pl-rim	Pl core	Pl incl in grt	Pl core
SiO_2	60.89	61.42	63.78	62.58	61.58	61.35	57.85	61.69
TiO_2	0.27	0.25	0.31	0.25	0.27	0.27	0.25	0.27
Al_2O_3	23.64	23.52	18.14	22.96	22.89	23.86	25.41	23.78
Cr_2O_3	0.13	0.10	0.09	0.10	0.12	0.12	0.12	0.13
FeO	0.20	0.19	0.14	0.15	0.18	0.19	0.42	0.16
MnO	0.12	0.13	0.13	0.14	0.13	0.14	0.12	0.12
MgO	0.07	0.07	0.08	0.08	0.08	0.08	0.08	0.06
CaO	5.47	5.76	0.38	4.65	4.76	6.08	7.92	6.57
Na_2O	8.61	8.57	2.13	9.10	8.79	8.46	7.30	8.18
K_2O	0.51	0.36	12.98	0.33	0.30	0.20	0.23	0.21
Total	99.91	100.36	98.18	100.33	99.09	100.75	99.70	101.17
Cations on the basis of 8 oxygen								
Si	2.720	2.729	2.978	2.771	2.761	2.716	2.606	2.720
Ti	0.009	0.008	0.011	0.008	0.009	0.009	0.008	0.009
Al	1.245	1.232	0.998	1.199	1.210	1.245	1.350	1.236
Cr	0.005	0.004	0.003	0.004	0.004	0.004	0.004	0.005
Fe	0.007	0.006	0.005	0.005	0.006	0.006	0.014	0.005
Mn	0.005	0.005	0.005	0.005	0.005	0.005	0.005	0.004
Mg	0.005	0.005	0.006	0.005	0.005	0.005	0.005	0.004
Ca	0.262	0.274	0.019	0.220	0.229	0.288	0.382	0.310
Na	0.745	0.738	0.193	0.781	0.764	0.726	0.638	0.699
K	0.029	0.020	0.774	0.019	0.017	0.011	0.013	0.012
Total	5.031	5.021	4.992	5.017	5.011	5.016	5.026	5.004
X_{An}	0.26	0.27	-	0.22	0.23	0.28	0.37	0.31

Table 7. Summary of pressure-temperature estimates based on conventional geothermobarometries.

Sample	Method	Calibration	T°C (at 8 kbar)	P kbar (at 800°C)
KG050103-03	Garnet-biotite	Ganguly and Saxena (1984)	670 - 755	
		Dasgupta *et al.* (1991)	705 - 735	
KG050103-03	Garnet-biotite	Ganguly and Saxena (1984)	710 - 770	
		Dasgupta *et al.* (1991)	685 - 735	
KG050103-12	Garnet-biotite	Ganguly and Saxena (1984)	660 - 750	
		Dasgupta *et al.* (1991)	680 - 770	
	GASP	Newton and Haselton (1981)		8.4 - 9.0
		Ganguly and Saxena (1984)		6.6 - 7.5
ST050103-11-1B	Garnet-biotite	Ganguly and Saxena (1984)	650 - 700	
		Dasgupta *et al.* (1991)	640 - 690	
	GASP	Newton and Haselton (1981)		7.5 - 9.6
		Ganguly and Saxena (1984)		6.1 - 8.0
ST050103-5-1C	Garnet-orthopyroxene	Sen and Bhattacharya (1984)	730 - 850	
		Lee and Ganguly (1988)	770 - 880	
	GOPQ	Newton and Perkins (1982)		7.5 - 9.1
		Bhattacharya (1981)		7.4 - 8.9

Table 6 (continued).

fsp 1-49	fsp 87	fsp 37	fsp 80	fsp 92	fsp 190	fsp 193	fsp 65	fsp 14
ST050103-5-1C	ST050103-11-1B	ST050103-11-1B	ST050103-12-2-2B	ST050103-12-2-2B	SU050104-03	SU050104-03	SU050104-08	SU050104-08
BR	BR	BR	BR	BR	GR	GR	GR	GR
Grt-Opx granulite	Grt-Bt-Sil-Gr gneiss	Grt-Bt-Sil-Gr gneiss	Amphibolite	Amphibolite	Grt-Bt gneiss	Grt-Bt gneiss	Amphibolite	Amphibolite
Pl rim	Pl core	Pl rim	Pl in opx	Pl rim matrix	matrix core	matrix rim	matrix	incl in grt
59.82	61.90	63.09	46.65	54.27	59.73	59.34	52.87	47.72
0.22	0.23	0.24	0.29	0.27	0.26	0.25	0.26	0.26
23.33	22.87	22.70	33.37	28.88	24.93	24.68	29.61	33.88
0.12	0.12	0.12	0.12	0.09	0.14	0.12	0.11	0.12
0.20	0.19	0.14	0.33	0.17	0.25	0.23	0.20	0.39
0.11	0.12	0.13	0.13	0.12	0.14	0.13	0.12	0.12
0.07	0.07	0.06	0.07	0.08	0.07	0.07	0.08	0.08
7.23	4.62	4.25	17.01	11.12	7.50	7.41	12.97	17.43
7.72	9.40	9.51	2.39	5.74	7.35	7.32	4.16	1.95
0.18	0.21	0.40	0.10	0.17	0.29	0.26	0.13	0.13
99.00	99.73	100.64	100.46	100.91	100.66	99.81	100.50	102.09
2.702	2.761	2.785	2.144	2.437	2.655	2.659	2.388	2.154
0.007	0.008	0.008	0.010	0.009	0.009	0.008	0.009	0.009
1.242	1.203	1.181	1.808	1.529	1.306	1.304	1.577	1.803
0.004	0.004	0.004	0.004	0.003	0.005	0.004	0.004	0.004
0.007	0.006	0.005	0.012	0.006	0.008	0.008	0.007	0.013
0.004	0.005	0.005	0.005	0.005	0.005	0.005	0.004	0.005
0.005	0.005	0.004	0.005	0.005	0.005	0.005	0.006	0.005
0.350	0.221	0.201	0.838	0.535	0.357	0.356	0.628	0.843
0.676	0.813	0.814	0.213	0.500	0.634	0.636	0.365	0.171
0.010	0.012	0.023	0.006	0.010	0.017	0.015	0.008	0.008
5.008	5.037	5.030	5.044	5.039	5.001	5.000	4.995	5.015
0.34	0.21	0.20	0.80	0.52	0.36	0.36	0.63	0.83

around 600°C at pressure of 4–5 kbar. Although these temperature estimates should be used cautiously because the diffusion rates are controlled by grain size and diffusion constants, a cooling dominated retrogression can well be assigned to the BR and GR rock units. The presence of kyanite mineral inclusions within garnet suggests a clockwise *P-T* path for the region. Kyanite inclusions are common in pelitic lithologies in the LHC (Hiroi *et al.,* 1983), which can be inferred as remnants of a clockwise *P-T* path. Subsequently, the BR and GR area also experienced a clockwise *P-T* path, similar to the regional metamorphic *P-T* evolution reported for LHC.

10.2. Implications for the regional geology of the Prince Olav Coast

Deformation events in high-grade metamorphic terranes are often difficult to constrain, especially in terrains that experienced partial melting. However, as observed in this study, competent basic lithologies help us in some extent to deduce the deforma-

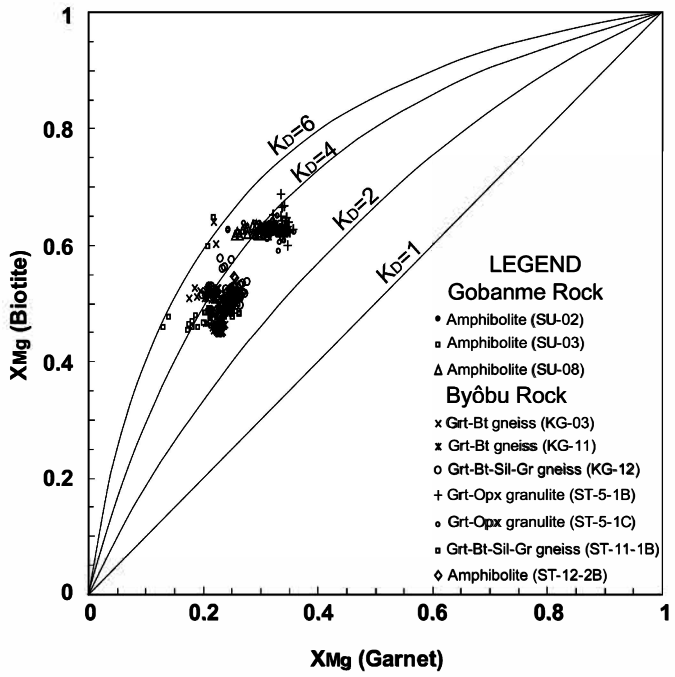

Fig. 12. *X_{Mg} relation between co-existing garnet and biotite. In spite of the variations in X_{Mg} contents in different rock units, they plot in a similar K_D line indication high pressure-temperature equilibrium conditions.*

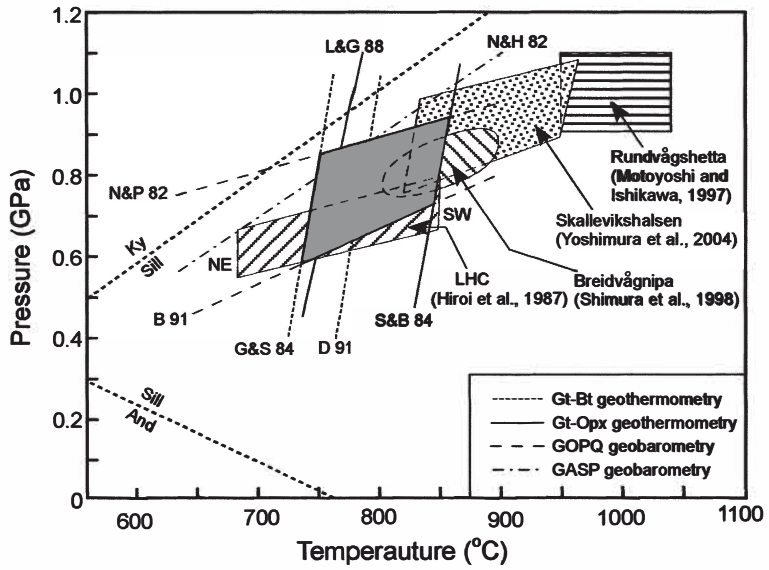

Fig. 13. *Metamorphic P-T estimates of BR and GR rock units based on various geothermo-barometries and a comparison with the reported P-T conditions in the Lützow-Holm Complex.*

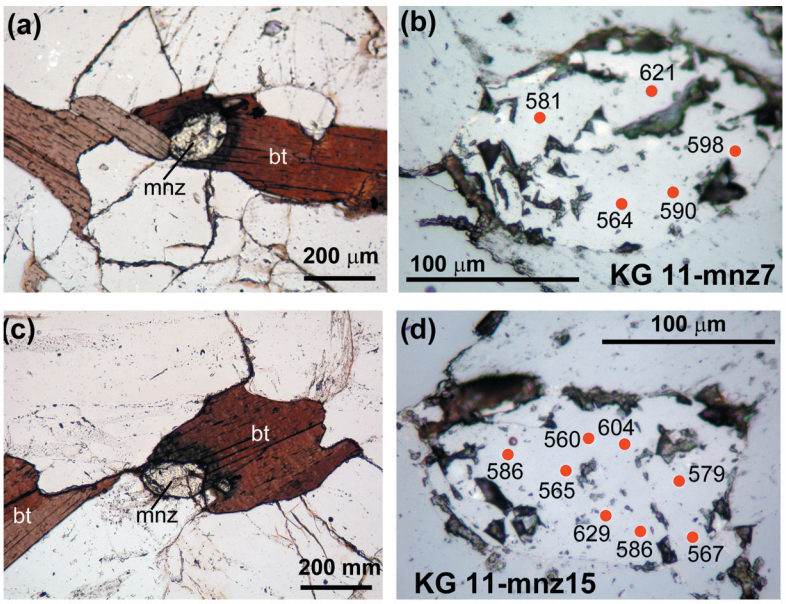

Fig. 14. Photomicrographs of monazite grains used for EMP dating. (a) and (c) Monazite grains in the matrix associated with biotite (plane polarized light) and (b) and (d) show the enlarged view of the monazite grain (under reflected light) with analyzed spots showing apparent chemical ages in Ma.

tion history. We have tentatively defined three major deformation events in Byôbu Rock and Gobanme Rock. The first one is the major phase of deformation resulting in the regional gneissosity, which follow an earlier folding event evidenced by the widespread occurrence of rootless tight isoclinal folds. The final phase of deformation identified is the regional gentle fold. In a recent study, Ikeda and Kawakami (2004) identified three phases of deformation from the Akarui Point in the Prince Olav Coast, which is ~30 km away from the BR. The first phase was associated with the formation of regional foliation which are locally parallel to the axial planes of isoclinal and intrafolial folds. A second phase of deformation identified in Akarui Point, produced crenulation lineation and axial planar foliation, whereas the last phase of deformation resulted in gentle open folds. These deformation events in the Akarui Point outcrop are probably synchronous with the deformation events observed in GR and BR outcrops. Shiraishi *et al.* (1983) described the deformation structures at Tenmondai Rock, where the regional foliation of the gneisses were trending NW-SE with dips between 40–85°SW. Further, Nishida *et al.* (1984) suggested the presence of a regional antiform, at Kasumi Rock, with an axial trace in the NNW-SSE direction. The data from these two neighboring outcrops to BR and GR are consistent with the regional trend of layering and folding observed in this study. Further field data as well as micro-structural data is necessary to understand the deformation history of this part of the Prince Olav Coast.

Granitic rocks in the LHC comprise of both syn and post metamorphic origin (e.g.

Shimura *et al.,* 1998; Ajishi *et al.,* 2004; Kawano *et al.,* 2005; Osanai *et al.,* 2004). Shimura *et al.* (1998) suggested anatexis of metapelitic rocks as the source for peraluminous granites in Breidvågnipa. However, the granitic rocks of Skallen region show wide geochemical variations with ASI values less than 1.1, which were interpreted to be derived from a source other than partial melting of adjacent pelitic gneisses (Osanai *et al.,* 2004). The mode of occurrence, petrologic characteristics and geochemical features of granitic rocks at BR suggests a role of anatexis, whereas those associated with amphibolites at GR does not clearly show any evidence of local origin of the magma. Therefore, further detail study on the geochemical characteristics of migmatites and granitic rocks is necessary to deduce the tectonic significance of intrusive rocks in the region.

The general geology of BR and GR is comparable with that of the adjoining exposures of Tenmondai Rock and Kasumi Rock in the Prince Olav Coast. Tenmondai Rock is underlain by well layered gneisses, migmatites and granitic rocks, with minor intercalations of amphibolites (Shiraishi *et al.,* 1985). The occurrence of kyanite inclusions in garnet is reported from this locality (Hiroi *et al.,* 1983), analogous to our finding at BR. Rare occurrence of orthopyroxene in this exposure was considered as the first in the metamorphic sequence from northeast to southwest of the LHC (Shiraishi *et al.,* 1984). A consistent foliation trend of NW-SE is observed in this outcrop. Apart from the numerous mesoscopic fold structures, a regional tight synform and an open antiform were reported in this outcrop (Shiraishi *et al.,* 1985). These geological features are identical to those observed in GR and BR exposures.

At Kasumi Rock exposure gneissic rocks are widely distributed with intercalations of marbles and amphibolites (Nishida *et al.,* 1984). Nishida *et al.* (1980) recognized a large scale antiform with an EW axis. Also, several mesoscopic steeply plunging recumbent folds were recognized. The structural and petrologic features of Kasumi Rock exposure closely resemble with the BR and GR outcrops, however Kasumi Rock have ubiquitous metacarbonate intercalations, which could not be identified in BR and GR.

In general, it can be concluded that the exposures from Tenmondai Rock to Kasumi Rock in the Prince Olav Coast have comparable geological features. However, there is local variation in lothfacies that suggest a shift from a metaigneous dominant one in the southwest to a metasedimentary dominant one in the northeast. Regional significance of this lithofacies distribution needs further attention in future.

10.3. Significance of monazite ages

As a whole, monazite ages from this study consist of a single population, irrespective of textural sites (Fig. 15). The distribution of this age population, having an average apparent age of 557 ± 33, can be considered as part of the Pan-African tectonothermal event. Several earlier studies have evidently pointed out that the main metamorphic event in the LHC occurred between 560–520 Ma, during the Pan-African orogeny (Shiraishi *et al.,* 1994, 2003; Fraser *et al.,* 2000, among others).

Shiraishi *et al.* (2003) reported 518 ± 12 Ma SHRIMP ages for zircons from a pelitic gneiss from Akarui Point, whereas a pelitic rock from Sinnan Rocks gave 553 ± 6 Ma.

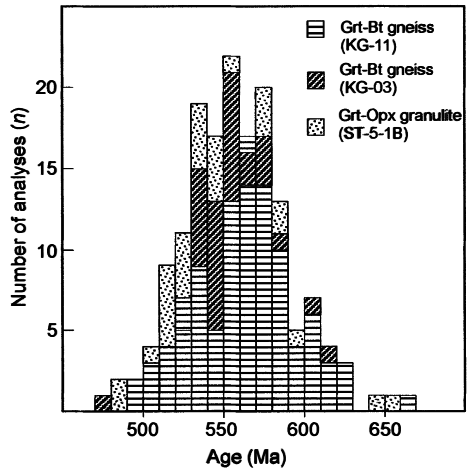

Fig. 15. Histogram of EMP monazite U-Th-Pb chemical ages obtained from Byôbu Rock samples.

Fraser (1997) proposed that the high-grade metamorphic conditions prevailed for at least 40 My in the LHC, based on extensive SHRIMP dating of zircon. This was further supported by a detail age determination using CHIME dating by Asami *et al.* (1997). Our results are within this range and in close agreement with the existing age data along the LHC. However, it remains a topic for future study, on the significance of the older ages near 550 Ma towards the eastern region of LHC, particularly in the Prince Olav Coast. Perhaps they suggest to a temporal gradient within the Pan-African tectonothermal event in the eastern Dronning Maud Land.

Acknowledgments

We thank Prof. Y. Hiroi and Dr. N. Ishikawa for constant support, encouragements and discussions during the JARE-46 field survey. We are indebted to Dr. T. Hokada for his kind helps in obtaining the EMP monazite ages and confirmation of kyanite using Laser Raman spectroscopy. Thanks are also due to JARE-46 members and "*Shirase*" crew for logistic support. We thank T. Ogino and M. Takai ("Little Blue" helicopter crew) for their valuable support in the successful completion of field survey at Byôbu Rock and Gobanme Rock. Drs. Y. Yoshimura and T. Shimura gave us valuable comments, which helped in improving the manuscript considerably. MS-K acknowledges grant from the Ministry of Education, Culture, Sports, Science and Technology, Japan (No.18740319).

References

Ajishi, H., Kawano, Y., Kawakami, T. and Ikeda, T. (2004): Geochronological study of post-metamorphic granite from Kasumi Rock, Lützow-Holm Complex, East Antarctica. Polar Geosci., **17**, 35–44.

Asami, M., Suzuki, K. and Adachi, M. (1997): Th, U and Pb analytical data and CHIME dating of monazites from metamorphic rocks of the Rayner, Lützow-Holm, Yamato-Belgica and Sør Rondane

Complexes, East Antarctica. Proc. NIPR Symp. Antarct. Geosci., **10**, 130–152.
Bence, A.E. and Albee, A.L. (1968): Empirical correction factors for the electron microanalysis of silicates and oxides. J. Geol., **76**, 382–403.
Bhattacharya, A., Krishnakumar, K.R., Raith, M. and Sen, S.K. (1991): An improved set of *a-X* parameters for Fe-Mg-Ca garnets and refinements of the orthopyroxene-garnet thermometer and the orthopyroxene-garnet-plagioclase-quartz barometer. J. Petrol., **32**, 629–656.
Dasgupta, S., Sengupta, P., Guha, D. and Fukuoka, M. (1991): A refined garnet-biotite Fe-Mg exchange geothermometer and its application in amphibolites and granulties. Contrib. Mineral. Petrol., **109**, 130–137.
Fraser, G. (1997): Geochronological constraints on the metamorphic evolution and exhumation of the Lützow-Holm Complex, East Antarctica. Ph. D. Thesis, The Australian National University, 254 p.
Fraser, G., McDougall, I., Ellis, D.J. and Williams, I. S. (2000): Timing and rate of isothermal decompression in Pan-African granulites from Rundvagashetta, East Antarctica. J. Metamorph. Geol., **18**, 441–454.
Ganguly, J. and Saxena, S. (1984): Mixing properties of alunminosilicate garnets: constraints from natural and experimental data, and applications to geothermo-barometry. Am. Mineral., **69**, 88–97.
Hiroi, Y., Shiraishi, K., Yanai, K. and Kizaki, K. (1983): Aluminum silicates in the Prince Olav and Sôya Coasts, East Antarctica. Mem. Natl Inst. Polar Res., Spec. Issue, **28**, 115–131.
Hiroi, Y., Shiraishi, K., Motoyoshi, Y., Kanisawa, S., Yanai, K. and Kizaki, K. (1986): Mode of occurrence, bulk chemical compositions, and mineral textures of ultramafic rocks in the Lützow-Holm Complex, East Antarctica. Mem. Natl Inst. Polar Res., Spec. Issue, **43**, 62–84.
Hiroi, Y., Shiraishi, K., Motoyoshi, Y. and Katsushima, T. (1987): Progressive metamorphism of calc-silicate rocks from the Prince Olav and Sôya Coasts, East Antarctica. Proc. NIPR Symp. Antarct. Geosci., **1**, 73–97.
Hokada, T., Misawa, K., Yokoyama, K., Shiraishi1, K. and Yamaguchi, A. (2004): SHRIMP and electron microprobe chronology of UHT metamorphism in the Napier Complex, East Antarctica: implications for zircon growth at $>1{,}000$℃. Contrib. Mineral. Petrol., **147**, 1–20.
Ikeda, T. and Kawakami, T. (2004): Structural analysis of Lützow-Holm Complex in Akarui Point, East Antarctica, and overview of the complex. Polar Geosci., **17**, 22–34.
Kawano, Y., Meno, A., Nishi, N. and Kagami, H. (2005): Geochemistry of the pre/syn-metamorphic granite in the Ongul Islands, East Antarctica. Polar Geosci., **18**, 114–129.
Kretz , R. (1983): Symbols for rock-forming minerals. Am. Mineral., **68**, 277–279.
Lawyer, L.A., Gahgan, L.M. and Dalziel, I.W.D. (1998): A tight-fit early Mesozoic Gondwana: a plate reconstruction perspective. Mem. Natl Inst. Polar Res., Spec. Issue, **53**, 214–229.
Leake, B.E., Woolley, A.R., Arps, C.E.S., Birch, W.D., Gilbert, M.C., Grice, J.D., Hawthorne, F.C., Kato, A., Kisch, H.J., Krivovichev, V.G., Linthout, K., Lard, J. and Mandarino, J. (1997): Nomenclature of amphiboles: report of the subcommittee of the international mineralogical association, commission on new minerals and mineral names. Mineral. Mag., **61**, 295–321.
Lee, H.Y. and Ganguly, J. (1988): Equilibrium compositions of coexisting garnet and orthopyroxene: Experimental determinations in the system FeO-MgO-Al_2O_3-SiO_2, and applications. J. Petrol., **29**, 93–113.
Motoyoshi, Y. and Ishikawa, M. (1997): Metamorphic and structural evolution of granulites from Rundvågshetta, Lützow-Holm Bay, East Antarctica. The Antarctic Region: Geological Evolution and Processes, ed. by C.A. Ricci. Siena, Terra Antarct. Publ., 65–72.
Motoyoshi, Y., Matsubara, S. and Matsueda, H. (1989): *P-T* evolution of the granulite-facies rocks of the Lützow-Holm Bay region, East Antarctica. Evolution of Metamorphic Belts, ed. by J.S. Daly *et al.* Oxford, Geological Society (London), 325–329 (Geol. Soc. Spec. Publ. **43**).
Nakamura, Y. and Kushiro, I. (1970): Equilibrium relations of hypersthene, pigeonite and augite in crystallizing magmas: microprobe study of a pigeonite andesite from Weiselberg, Germany. Am. Mineral., **55**, 1999–2015.
Newton, R.C. and Haselton, H.T. (1981): Thermodynamics of the garnet-plagioclase-Al_2SiO_5-quartz geobarometer. Thermodynamics of Minerals and Melts, ed. by R.C. Newton *et al.* New York, Springer, 131–147.
Newton, R.C. and Perkins, D. (1982): Thermodynamic calibration of geobarometers based on the assemblage

garnet-plagioclase-orthopyroxene (clinopyroxene)-quartz. Am. Mineral., **69**, 203–222.
Nishida, T., Yanai, K. and Kojima, H. (1980): Geology of Kasumi Rock, East Antarctica. Mem. Natl Inst. Polar Res., Spec. Issue, **21**, 1–9.
Nishida, T., Yanai, K., Kojima, H., Matsueda, H. and Kanisawa, S. (1984): Geological map of Kasumi Rock, Antarctica. Antarctic Geological Map Series, Sheet 18 (with explanatory text 6 p.). Tokyo, Natl Inst. Polar Res.
Osanai, Y., Toyoshima, T., Owada, M., Tsunogae, T., Hokada T., Crowe, W.A., Ikeda, T., Kawakami, T., Kawano, Y., Kawasaki, T., Ishikawa, M., Motoyoshi, Y. and Shiraishi, K. (2004): Geological map of Skallen, East Antarctica (revised version). Antarctic Geological Map Series, Sheet 39 (with explanatory text 23 p.) Tokyo, Natl Inst. Polar Res.
Pattison, D.R.M., Chacko, T., Farquhar, J. and McFarlane, C.R.M. (2003): Temperatures of granulite-facies metamorphism: Constraints from experimental phase equilibria and thermobarometry corrected for retrograde exchange. J. Petrol., **44**, 867–900.
Pearce, J., Harris, N.B.W. and Tindle, A.G. (1984): Trace element discrimination diagrams for tectonic interpretation of granitic rock. J. Petrol., **25**, 956–983.
Sen, S.K. and Bhattacharya, A. (1984): An orthopyroxene-garnet geothermometer and its application to the Madras charnockites. Contrib. Mineral. Petrol., **88**, 64–71.
Shimura, T., Fraser, G.L., Tsuchiya, N. and Kagami, H. (1998): Genesis of the migmatites of Breidvågnipa, East Antarctica. Mem. Natl Inst. Polar Res., Spec. Issue, **53**, 109–136.
Shiraishi, K., Hiroi, Y., Sasaki, K., Yanai, K. and Kizaki, K. (1983): Geological structure of the Prince Olav Coast. The 4th Symposium on Antarctic Geosciences, Program and Abstracts, 28–29 October 1983. Tokyo, Natl Inst. Polar Res. 79-80 (in Japanese).
Shiraishi, K., Hiroi, Y. and Onuki, H. (1984): Orthopyroxene-bearing rocks from the Tenmondai and Naga-Iwa Rocks in the Prince Olav Coast, East Antarctica: First appearance of orthopyroxene in the progressive metamorphic sequence. Mem. Natl Inst. Polar Res., Spec. Issue, **33**, 126–144.
Shiraishi, K., Hiroi, Y., Moriwaki, K., Sasaki, K. and Onuki, H. (1985): Geological map of Tenmondai Rock, Antarctica. Antarctic Geological Map Series, Sheet 19 (with explanatory text 7 p.). Tokyo, Natl Inst. Polar Res.
Shiraishi, K., Ellis, D.J., Hiroi, Y., Fanning, C.M., Motoyoshi, Y. and Nakai, Y. (1994): Cambrian orogenic belt in East Antarctica and Sri Lanka: Implications for Gondwana assembly. J. Geol., **102**, 47–65.
Shiraishi, K., Hokada, T., Fanning, C.M., Misawa, K. and Motoyoshi, Y. (2003): Timing of thermal events in eastern Dronning Maud Land, East Antarctica. Polar Geosci., **16**, 76–99.
Spear, F.S. (1991): On the interpretation of peak metamorphic temperatures in light of garnet diffusion during cooling. J. Metamorph. Geol., **9**, 379–388.
Spear, F.S. and Florence, F.P. (1992): Thermobarometry in granulites: pitfalls and new approaches. Precambrian Res., **55**, 209–241.
Streckeisen, A. (1976): To each plutonic rock its proper name. Earth Sci. Rev., **12**, 1–33.
Yoshida, M. (1995): Assembly of East Gondwanaland during the Mesoproterozoic and its rejuvenation during the Pan-African period. India and Antarctica during the Precambrian, ed. by M. Yoshida and M. Santosh. Geol. Soc. India, Mem., **34**, 25–45.
Yoshimura, Y., Motoyoshi, Y., Miyamoto, T., Grew, E.S., Carson, C.J. and Dunkley, D.J. (2004): High-grade metamorphic rocks from Skallevikshalsen in the Lützow-Holm Complex, East Antarctica: Metamorphic conditions and possibility of partial melting. Polar Geosci., **17**, 57–88.

Appendix 1. Electron microprobe analytical results of monazite and U-Th-Pb ages for Byôbu Rock samples.

	Age (Ma)	error (Ma)	UO_2 (wt%)	ThO_2 (wt%)	UO_2* (wt%)	ThO_2* (wt%)	PbO (wt%)	Th/U
KG05010311								
mnz1.1	549	30	0.570	4.370	1.943	6.263	0.146	7.83
mnz1.2	566	28	0.606	4.710	2.086	6.724	0.161	7.95
mnz1.3	571	31	0.543	4.230	1.871	6.034	0.146	7.97
mnz1.4	557	30	0.586	4.310	1.940	6.255	0.148	7.52
mnz2.1	528	29	0.522	4.630	1.976	6.359	0.142	9.07
mnz2.2	538	31	0.431	4.530	1.854	5.958	0.136	10.75
mnz2.3	536	34	0.676	3.420	1.750	5.659	0.129	5.18
mnz2.4	530	30	0.551	4.460	1.951	6.284	0.141	8.28
mnz2.5	495	37	0.524	3.320	1.567	5.052	0.106	6.47
mnz3.1	545	31	0.549	4.290	1.897	6.112	0.141	7.99
mnz3.2	561	30	0.566	4.370	1.939	6.251	0.149	7.89
mnz3.3	513	33	0.589	3.820	1.789	5.767	0.125	6.64
mnz3.4	546	45	0.431	2.750	1.295	4.179	0.097	6.53
mnz3.5	584	44	0.431	2.860	1.329	4.293	0.106	6.79
mnz3.6	560	31	0.527	4.240	1.858	5.989	0.142	8.23
mnz3.7	553	44	0.437	2.840	1.329	4.290	0.101	6.65
mnz3.8	614	41	0.426	3.150	1.415	4.571	0.119	7.56
mnz3.9	512	30	0.522	4.430	1.913	6.156	0.133	8.68
mnz3.10	552	31	0.534	4.260	1.872	6.030	0.141	8.17
mnz4.1	510	31	0.512	4.260	1.850	5.952	0.129	8.52
mnz4.2	569	37	0.496	3.480	1.589	5.128	0.124	7.18
mnz4.3	498	33	0.485	3.990	1.738	5.593	0.118	8.41
mnz4.4	555	30	0.556	4.320	1.913	6.165	0.145	7.95
mnz5.1	583	36	0.458	3.690	1.617	5.213	0.129	8.24
mnz5.2	576	34	0.456	4.040	1.725	5.555	0.136	9.07
mnz5.3	511	30	0.561	4.300	1.912	6.156	0.133	7.84
mnz5.4	555	33	0.484	4.070	1.763	5.678	0.134	8.59
mnz5.5	608	33	0.472	4.170	1.782	5.744	0.148	9.03
mnz6.1	553	30	0.590	4.380	1.966	6.339	0.149	7.59
mnz6.2	574	33	0.546	3.860	1.759	5.676	0.138	7.23
mnz6.3	533	29	0.596	4.520	2.016	6.495	0.147	7.76
mnz6.4	570	30	0.551	4.330	1.911	6.161	0.149	8.04
mnz7.1	590	36	0.500	3.590	1.627	5.254	0.132	7.34
mnz7.2	564	38	0.444	3.510	1.546	4.984	0.119	8.09
mnz7.3	581	38	0.484	3.410	1.555	5.018	0.124	7.21
mnz7.4	621	30	0.632	4.300	1.983	6.409	0.169	6.96
mnz7.5	598	33	0.643	3.590	1.770	5.731	0.145	5.71
mnz8.1	569	30	0.823	3.620	1.960	6.353	0.153	4.50
mnz8.2	532	40	0.466	3.170	1.462	4.713	0.106	6.96
mnz8.3	551	37	0.515	3.330	1.561	5.040	0.118	6.61
mnz8.4	560	32	0.728	3.570	1.849	5.987	0.142	5.01
mnz8.5	577	31	0.465	4.400	1.847	5.947	0.145	9.67
mnz9.1	610	38	0.493	3.320	1.536	4.965	0.129	6.88
mnz9.2	608	38	0.475	3.370	1.533	4.953	0.128	7.26
mnz9.3	564	40	0.501	3.100	1.474	4.763	0.114	6.33
mnz9.4	584	38	0.504	3.280	1.534	4.956	0.123	6.66
mnz10.1	619	40	0.477	3.120	1.457	4.712	0.124	6.68
mnz10.2	573	37	0.529	3.410	1.600	5.167	0.126	6.60
mnz10.3	621	40	0.437	3.210	1.445	4.666	0.123	7.52
mnz10.4	572	30	0.624	4.290	1.972	6.365	0.154	7.03
mnz11.1	576	31	0.585	4.220	1.910	6.165	0.151	7.38
mnz11.2	569	31	0.576	4.170	1.886	6.085	0.147	7.40
mnz11.3	550	33	0.497	4.040	1.766	5.688	0.133	8.32
mnz11.4	532	38	0.489	3.310	1.528	4.929	0.111	6.93

Appendix 1 (continued).

	Age (Ma)	error (Ma)	UO2 (wt%)	ThO2 (wt%)	UO2* (wt%)	ThO2* (wt%)	PbO (wt%)	Th/U
mnz11.5	587	31	0.585	4.100	1.873	6.047	0.151	7.17
mnz12.1	544	40	0.429	3.240	1.447	4.663	0.107	7.72
mnz12.2	595	38	0.442	3.520	1.547	4.990	0.126	8.15
mnz12.3	520	30	0.561	4.370	1.934	6.228	0.137	7.96
mnz12.4	579	34	0.508	3.830	1.711	5.518	0.135	7.72
mnz12.5	501	31	0.547	4.150	1.850	5.956	0.126	7.77
mnz12.6	531	30	0.592	4.390	1.971	6.352	0.143	7.58
mnz12.7	501	36	0.604	3.300	1.640	5.295	0.112	5.59
mnz12.8	509	31	0.540	4.260	1.878	6.044	0.130	8.08
mnz13.1	574	35	0.514	3.730	1.685	5.437	0.132	7.43
mnz13.2	568	33	0.637	3.600	1.768	5.716	0.138	5.78
mnz13.3	538	38	0.509	3.260	1.533	4.947	0.113	6.55
mnz13.4	570	34	0.583	3.610	1.717	5.546	0.134	6.34
mnz13.5	529	35	0.554	3.580	1.678	5.415	0.121	6.61
mnz14.1	587	36	0.488	3.660	1.638	5.285	0.132	7.67
mnz14.2	601	32	0.495	4.200	1.814	5.849	0.149	8.68
mnz14.3	542	31	0.532	4.260	1.870	6.022	0.138	8.20
mnz14.4	577	34	0.463	4.050	1.735	5.588	0.137	8.96
mnz14.5	555	31	0.578	4.240	1.909	6.157	0.145	7.51
mnz14.6	571	31	0.560	4.200	1.879	6.061	0.147	7.67
mnz14.7	603	31	0.569	4.190	1.885	6.086	0.156	7.53
mnz14.8	553	31	0.552	4.190	1.868	6.022	0.141	7.76
mnz15.1	604	32	0.562	4.010	1.821	5.882	0.151	7.30
mnz15.2	579	36	0.515	3.560	1.633	5.273	0.130	7.07
mnz15.3	567	30	0.803	3.670	1.956	6.338	0.152	4.67
mnz15.4	586	29	0.623	4.330	1.983	6.402	0.159	7.11
mnz15.5	629	37	0.445	3.600	1.576	5.085	0.136	8.28
mnz15.6	560	29	0.598	4.520	2.018	6.506	0.155	7.73
mnz15.7	565	33	0.540	3.970	1.787	5.765	0.138	7.51
mnz15.8	586	42	0.419	3.090	1.389	4.483	0.111	7.55
mnz16.1	552	30	0.524	4.550	1.953	6.288	0.147	8.88
mnz16.2	556	28	0.545	4.970	2.106	6.778	0.160	9.33
mnz16.3	533	30	0.550	4.510	1.967	6.333	0.143	8.38
mnz17.1	524	31	0.546	4.330	1.906	6.137	0.136	8.11
mnz17.2	583	33	0.399	4.250	1.734	5.576	0.138	10.90
mnz17.3	594	39	0.473	3.300	1.509	4.874	0.123	7.14
mnz17.4	580	35	0.524	3.680	1.680	5.423	0.133	7.18
mnz17.5	566	42	0.443	3.040	1.398	4.512	0.108	7.02
mnz17.6	605	35	0.511	3.760	1.692	5.464	0.140	7.52
mnz17.7	663	45	0.429	2.760	1.296	4.196	0.118	6.58
mnz17.8	555	29	0.599	4.500	2.013	6.489	0.153	7.68
mnz17.9	527	32	0.475	4.320	1.832	5.893	0.132	9.30
KG05010303								
mnz1.1	557	28	0.873	4.040	2.142	6.937	0.164	4.73
mnz1.2	542	23	0.835	5.520	2.568	8.287	0.191	6.76
mnz1.3	537	28	0.839	4.080	2.121	6.861	0.156	4.97
mnz1.4	534	29	0.662	4.360	2.031	6.552	0.148	6.74
mnz1.5	542	30	0.660	4.180	1.973	6.369	0.146	6.47
mnz2.1	566	24	0.674	5.530	2.411	7.771	0.186	8.39
mnz2.2	558	27	0.696	4.780	2.197	7.089	0.168	7.03
mnz2.3	551	24	0.873	4.950	2.428	7.847	0.183	5.80
mnz3.1	539	27	0.773	4.500	2.187	7.063	0.161	5.95
mnz3.2	533	26	0.739	4.750	2.231	7.198	0.163	6.57
mnz3.3	531	25	0.859	4.830	2.376	7.676	0.173	5.75
mnz3.4	479	25	0.700	5.200	2.333	7.508	0.152	7.60

Appendix 1 (continued).

	Age (Ma)	error (Ma)	UO2 (wt%)	ThO2 (wt%)	UO2* (wt%)	ThO2* (wt%)	PbO (wt%)	Th/U
mnz4.1	578	37	0.548	3.290	1.581	5.111	0.125	6.14
mnz4.2	555	22	0.876	5.590	2.632	8.497	0.200	6.53
mnz4.3	552	39	0.572	3.040	1.527	4.938	0.115	5.43
mnz4.4	540	31	0.678	3.800	1.871	6.047	0.138	5.73
mnz4.5	549	32	0.639	3.800	1.832	5.920	0.138	6.08
mnz5.1	615	44	0.407	2.910	1.321	4.269	0.111	7.31
mnz5.2	606	31	0.589	4.050	1.861	6.011	0.155	7.04
mnz5.3	538	27	0.518	5.300	2.182	7.016	0.160	10.47
mnz5.4	541	34	0.527	3.810	1.723	5.557	0.128	7.40
mnz5.5	547	42	0.464	3.000	1.406	4.537	0.105	6.62
mnz6.1	549	35	0.659	3.300	1.695	5.485	0.128	5.12
mnz6.2	585	40	0.508	3.100	1.481	4.789	0.119	6.25
mnz6.3	552	41	0.471	3.060	1.432	4.623	0.108	6.65
mnz6.4	524	47	0.436	2.600	1.253	4.045	0.090	6.09
mnz6.5	554	32	0.663	3.650	1.810	5.851	0.138	5.63
mnz7.1	547	34	0.575	3.580	1.699	5.487	0.127	6.37
mnz7.2	575	29	0.611	4.380	1.987	6.412	0.156	7.33
mnz7.3	578	31	0.681	3.860	1.894	6.125	0.150	5.79
mnz8.1	550	25	0.639	5.510	2.369	7.629	0.178	8.82
mnz8.2	538	27	0.717	4.630	2.171	7.007	0.160	6.60
mnz8.3	569	32	0.606	3.900	1.831	5.913	0.143	6.58
mnz8.4	525	36	0.479	3.630	1.619	5.214	0.116	7.76
ST050103-5-1B-2								
mnz1.1	535	44	0.468	2.750	1.332	4.300	0.097	6.01
mnz1.2	549	39	0.298	3.780	1.485	4.769	0.111	12.97
mnz1.3	519	44	0.453	2.800	1.333	4.301	0.095	6.32
mnz1.4	526	44	0.447	2.810	1.330	4.291	0.096	6.42
mnz1.5	585	71	0.646	0.711	0.870	2.861	0.071	1.13
mnz1.6	528	37	0.395	3.720	1.563	5.027	0.113	9.64
mnz1.7	578	28	0.195	5.820	2.023	6.467	0.159	30.57
mnz1.8	544	34	0.214	4.720	1.697	5.430	0.125	22.54
mnz1.9	582	47	0.200	3.260	1.224	3.925	0.097	16.67
mnz2.1	646	74	0.273	1.640	0.789	2.554	0.070	6.13
mnz2.2	659	88	0.189	1.500	0.660	2.132	0.060	8.13
mnz2.3	579	66	0.258	2.000	0.886	2.858	0.070	7.93
mnz2.4	481	62	0.220	2.250	0.926	2.975	0.061	10.48
mnz3.1	563	41	0.283	3.550	1.398	4.491	0.107	12.82
mnz3.2	501	48	0.237	3.040	1.192	3.824	0.081	13.11
mnz3.3	540	54	0.185	2.810	1.068	3.424	0.078	15.51
mnz3.4	551	49	0.199	3.070	1.163	3.730	0.087	15.79
mnz4.1.	517	38	0.521	3.210	1.529	4.932	0.108	6.31
mnz4.2	488	52	0.214	2.840	1.106	3.547	0.073	13.57
mnz4.3	513	53	0.583	1.760	1.136	3.690	0.080	3.09
mnz4.4	529	48	0.290	2.950	1.217	3.910	0.088	10.40
mnz4.5	534	35	0.352	4.160	1.659	5.328	0.121	12.07
mnz5.1	591	39	0.203	4.090	1.488	4.766	0.119	20.59
mnz5.2	574	45	0.212	3.430	1.290	4.136	0.101	16.51
mnz5.3	540	34	0.283	4.430	1.674	5.368	0.123	16.01
mnz6.1	533	29	0.205	5.690	1.992	6.369	0.144	28.39
mnz6.2	534	53	0.187	2.890	1.094	3.508	0.079	15.84
mnz6.3	528	47	0.712	1.760	1.265	4.119	0.092	2.53
mnz6.4	514	31	0.269	5.030	1.849	5.921	0.129	19.11
mnz6.5	518	30	0.193	5.520	1.926	6.157	0.135	29.32